A Computational Investigation of Bio-Inspired Formation Flight and Ground Effect

David J. Willis *, Jaime Peraire †, Kenneth S. Breuer‡

Energy saving strategies such as formation flight and near-ground flight are frequently exploited in nature. The energy reduction mechanisms of these approaches are conceptually simple; however, the unsteady wake vortex structures that result from flapping may provide additional benefits. Since these flight strategies offer increased energy savings over simple flight situations, they have received much attention from both the biological sciences and engineering research communities; however, these analysis have traditionally been restricted to the steady aerodynamics of rigid wing vehicles. In this paper, we present a preliminary computational study of energy saving strategies in flapping flight. In both formation flight and ground effect flight, beneficial energy savings are predicted. In the case of formation flight, optimal savings are predicted to occur when the unsteady wake vorticity is exploited by ensuring that the two flappers' wakes are in spatial phase with wingtips slightly overlapping.

I. Introduction

Migrations are costly and often require that birds and bats invoke flight strategies or behaviors which maximize the chances of survival.[1,2] In nature, aerodynamic strategies which appear to reduce flight energy consumption are commonly observed in birds undergoing long migrations.[2–4] Of these energy reduction strategies, two of the more commonly exploited and examined approaches are formation flight[3,5,7–9,11,40] and flight near the ground or water surfaces.[7,8,12,27] Although it is commonly accepted that birds[13–17] and bats[18] exploit ground effect energy savings, there is still some contention about the degree of exploitation of vortex structure flow energy in formation flight. Several authors[19–21] have suggested visual and communication factors may play a significant role in the flocking arrangement and behavior, and thus the actual energy savings may be significantly below the theoretical optimum. Furthermore, it has also been noted that certain flocking or grouping arrangements may be more suited to behavioral responses than others (such as group protection and predator evasion).[19] Aerodynamically, both ground effect and formation flight can minimize the required flight energy by exploiting or reducing the adverse induced effects of wing-trailing vortex systems. The induced drag or drag due to lift has been presented and reviewed in many different references.[57,59–61]

Unlike aircraft, where the thrust and lift generation are decoupled, birds, bats and fish predominantly exploit a single lifting surface for most of their active force generation. This flight and propulsion strategy generates a single pseudo-periodic wake containing regions of both low and high span-wise and stream-wise vorticity. As a result of this complex wake vorticity distribution, we hypothesize that induced drag and induced power savings in formation and ground effect flapping flight may be higher than those savings attainable by similarly scaled fixed wing aircraft. In much of the literature addressing quantitative assessments of induced power saving mechanisms, the lift generation is assumed to be time-invariant and produced by a rigid wing.[23–25,27] This assumption is likely valid for situations where the wing does not undergo significant time-dependent morphing (due to flapping) or in flight situations where thrust generation is minimal. The primary purpose of this study is not centered at accurately predicting and reporting the energy savings, but rather, it is directed at understanding the basic trends and considerations for higher fidelity, more robust simulations. In this paper, a preliminary low fidelity investigation of the energy savings is presented.

*Postdoctoral Research Associate, Department of Aeronautics and Astronautics, MIT
†Professor, Department of Aeronautics and Astronautics, MIT
‡Professor, Division of Engineering, Brown University.

I..1. Introduction to savings by ground effect

Flight in the presence of a ground plane (ground effect) has been a topic of interest due to the potential for significant energy savings.[25–27] In particular, these extreme energy savings have been investigated for rapid, large, over surface transport vehicles.[28,29] Not only has the ground effect phenomenon been of interest to vehicle designers, it has also been of interest to researchers trying to unlock the wonders of natural flight.[27]

The aerodynamically-solid ground plane acts as a resistance plane to the propagation of wake induced downwash effects over the wing section.[27,57] As a result of the reduced downwash on the wing, induced drag due to lift is subsequently lessened. Since ground effect savings are a function of the distance from the ground, typically energy savings only become noticeable when the lifting surface is within one span-length of the ground plane. In addition, since the flow around the wing section is altered by the presence of the ground plane, at small wing-ground separation, both the drag and lift may be affected. Analysis of these effects is neglected in the simple model which is considered and left for higher fidelity approaches. Rigid wings generating lift in proximity to the ground have been studied by several authors, all predicting the benefits of the ground plane on energy reduction.[25,32–34]

For flapping vehicles, the ground effect phenomenon may result in enhanced energy savings due to the non-uniform position of the wing stations relative to the ground as well as the unsteady vorticity shedding from the trailing edge of the wing. Several authors have investigated the possible exploitation of unsteady flapping in ground effect.[22,34] Notably, Platzer and Jones[34] explored novel flapping propulsion techniques mimicking ground effect or mirror plane approaches using 2-dimensional airfoils. In this paper we examine the ground effect phenomenon in flapping flight and determine the general rules which might aid in the design of MAV's and UAV's using both flapping and ground effect strategies.

I..2. Introduction to savings by formation flight

Vortex capture is an elegant flow energy extraction mechanism which is exploited by nature and has also been pursued in engineered systems.[37,38] Formation flight in migratory birds and aircraft is an example of extracting the flow kinetic energy resident in the wake of a lifting surface. Traditionally, this energy savings is accomplished by a following vehicle appropriately capturing the wingtip vortices shed by a leading vehicle.[4] As early as the 1920s[42] approximations of the energy savings due to formation flight have been examined. By examining the rigid wing problem,[23,39–41] it is clear that significant energy reduction is possible when the following vehicle is located in the wing-outboard-upwash of the lead aircraft's vortex wake system. Furthermore, computations have also been able to explore the formation arrangements which are most favorable for the entire group.[23,25,35] This has lead to predictions of the energy savings possible in both energy reduction strategies.[23–25,33,36] One of the remaining challenges in understanding migratory flight resides in the need to represent the unsteady effects of single surface lift and thrust generation during flapping while considering the large dimensional design space. In this paper, we take a first step in understanding those effects using simplified models of the complex system.

For the formation flight problem, we examine the energy savings with respect to basic positioning and wing beat phase relationships between a leading bird and a following bird. We do not address or consider the optimal formation shape (eg. V-shaped) or the detailed modifications to the flapping kinematics or wing shapes which are needed for full exploitation of the wake vorticity. One might expect that, if unsteady effects were of significant importance in formation flight energy savings, that birds would exhibit some preference to frequency and phase locking in migratory formations. Although a small collection of authors have predicted or reported observing some preferred phase relationship,[43,44] many others have reported the opposite, namely there was no noticeable wing-beat locking or phase consistency between members of the formation.[45] As such, this study investigates the advantages of wing beat phase matching and how sensitive the flight of flapping vehicles is to this phase locking.

I..3. Introduction to the current analysis

This paper takes preliminary steps at examining the effects of non-steady vorticity wake structures in the energy saving scenarios of ground effect and migratory flight. We aim to gain insight into the salient features of these energy saving mechanisms by making simple analysis of the flow and flight. Since the flapping flight design space is so large, several simplifications are made to make even this preliminary analysis feasible. The first assumption is that the flappers will tend to produce nearly optimal wake circulation distributions for the particular situation in which they fly. This assumption may prove to be misleading as there are no

guarantees in nature or engineering that this is indeed possible or plausible. The second assumption which is made, relates closely to the first, namely, that the wake shape is a simple harmonic motion. This is clearly not the situation. The third main assumption is to perform much of the analysis we use a wake only optimal vorticity distribution solver similar to that proposed by Hall et al.[49–51] This assumption relies on the wake as being an adequate descriptor of potential body-to-body interactions. As such, this assumption limits the potential analysis and conclusions which can be drawn to more general and ideal cases. Although this may seem to be a significant drawback, understanding the trends and behavior of these simple systems is necessary prior to more robust computations.

II. Numerical Methods

In this preliminary study of energy savings, the wake only analysis presented by Hall et al.[49–51] is modified to capture the desired representation of the problem.

II.A. The *HallOpt* Wake Only Method

The use of wake only methods has become a common starting point for aerodynamics analysis,[59] experiment[37,54–56] and computation.[49,52,57] Since the wake contains details of the force generation history, it in effect acts as a footprint for that vehicle. For this study, HallOpt, an implementation of the wake only method of Hall et al.[49–51] is used with some minor modifications to account for ground planes and multiple flight vehicles. These particular modifications do not introduce any additional fundamental physics into the solution methodology. As a result only a brief review of the wake only process is performed in this paper, and the reader is referred to the original work of Hall et al.[49–51]

II.A.1. Review of Hall et al.'s Wake Only Method For Single Flapping Wings

In the method of Hall et al[49–51] the wake shed by a flapping vehicle is assumed to be infinitely periodic in the flight direction. A single period of this wake is selected and the optimal circulation distribution for that particular wake is determined. The following steps highlight the general solution process:

- A single period of the infinitely periodic wake trace surface is defined. This wake trace can be defined as the location of the trailing edge as it passes through the still air reference domain.
- The wake shape is discretized using a vortex lattice.[58]
- First order force constraints and viscous drag polar details are expressed as functions of the yet unknown wake vorticity. See equation 1.
- The minimum total power vorticity distribution is expressed as a constrained optimization problem whose minimum is determined using a linear system solve.

II.A.2. Wake Only: Accounting for Forces

The generation of first order forces is directly related to the circulation distribution and the shape of the wake:

$$\vec{F_1} = \frac{\rho}{T} \int_{WS} \Gamma \cdot \hat{n} dS \tag{1}$$

Here, ρ is the density, T is the flapping period, WS represents the wake surface, Γ represents the unknown wake circulation, $\hat{n}$ represents the normal at the wake point, and F_1 represents the first order forces. Note, that in the computation of the thrust and lift forces, there is no accounting for the induced velocity due to the vorticity in the wake.

II.A.3. Wake Only: Accounting for Power

The power required to create the particular wake vorticity distribution is composed of an induced power contribution (related to the vorticity induced losses) and a viscous contribution (due to the viscosity in the fluid, which can, through the original expressions,[50] be related to the circulation distribution in the wake). Although in this particular application, the induced losses are of most interest, the viscous terms are also

considered to provide realistic viscous bounds on the problem. The power consumption for a particular wake shape is:

$$P = P_i + P_{v1} + P_{v2} = -\frac{\rho}{2T}\int_{WS}\Delta\phi\nabla\phi\cdot\hat{n}dS + \frac{\rho}{2T}\int_{WS}\left(\frac{4C_{d2}}{c}\right)(\Gamma-\Gamma_0)^2 dS + \frac{\rho}{2T}\int_{WS}(U^2 cC_{d0})\cdot\left(\frac{ds}{dx}\right)^2 dS \tag{2}$$

To determine the wake circulation which minimizes the power in the wake, the constrained optimization problem is solved. The force constraints are added to the relationship for the power through a set of Lagrange multipliers. The minimum power circulation distribution can be determined by solving the resulting linear system.[49]

II.A.4. Wake Only Method For Multiple Wakes

In this section, the modifications necessary to model multiple wakes are presented. In this paper, both the formation flight and ground effect problem are analyzed using two wakes. It is possible to use more than two wakes, however, the analysis and results become slightly more challenging with little added benefit in the results. Starting from the Lagrangian power expression in matrix form (equation (37) of Hall et al.[50]):

$$\Pi = \frac{1}{2}\Gamma^T K\Gamma - \Gamma^T Q + \lambda^T\left(B\Gamma - F_R\right) + P_{v0}, \tag{3}$$

the power can be predicted as a function of the unknown circulation distribution in the wake. This power represents the flow energy and viscous effects inside a one period region of the wake. There is no limitation on either the shape or the number of wakes in the domain which is being analyzed. This means that the above equation may represent more than one wake surface in the domain of interest.

Potential flow vortex lattice methods[58] are used to discretize the aerodynamic influence matrix (K) in HallOpt. The vorticity representation is one of discrete rings (or constant potential jump doublet panels), however, in the future we plan to increase the order of the representation in order to gain the benefits of a less singular vortex sheet arrangement.

The goal of the analysis is to explore multiple wake arrangements in space. Since the interesting features of multiple wake flight lie in the induced power savings, we neglect the viscous terms for the remainder of the derivation (for simplicity, they can be and are incorporated in simulations of ground effect and formation flight). Therefore, the expression for the Lagrangian power is:

$$\Pi = \frac{1}{2}\Gamma^T K\Gamma + \lambda^T\left(B\Gamma - F_R\right) \tag{4}$$

If two wakes are considered, the matrix system, written out in detail is:

$$\Pi = \frac{1}{2}\begin{bmatrix}\Gamma_1\\ \Gamma_2\end{bmatrix}^T\begin{bmatrix}K_{11} & K_{12}\\ K_{21} & K_{22}\end{bmatrix}\begin{bmatrix}\Gamma_1\\ \Gamma_2\end{bmatrix} + \begin{bmatrix}\lambda_1\\ \lambda_2\end{bmatrix}^T\left(\begin{bmatrix}B_{1x} & 0\\ B_{1_y} & 0\\ B_{1z} & 0\\ 0 & B_{2x}\\ 0 & B_{2y}\\ 0 & B_{2z}\end{bmatrix}\begin{bmatrix}\Gamma_1\\ \Gamma_2\end{bmatrix} - \begin{bmatrix}F_{R_{1x}}\\ F_{R_{1y}}\\ F_{R_{1z}}\\ F_{R_{2x}}\\ F_{R_{2y}}\\ F_{R_{2z}}\end{bmatrix}\right) \tag{5}$$

In the above matrix equation, the subscript 1 refers to wake number 1, and the subscript 2 refers to the second wake. In the influence matrix K, K_{xx} refers to the wake induced by a wake on itself, while K_{xy} represents the cross-influence between wakes. The matrix system is then expanded into components which represent particular interactions in the system:

$$\Pi = \frac{1}{2}\left(\Gamma_1^T K_{11}\Gamma_1 + \left(\Gamma_1^T K_{12}\Gamma_2 + \Gamma_2^T K_{21}\Gamma_1\right) + \Gamma_2^T K_{22}\Gamma_2\right) + \lambda_1^T\left(B_1\Gamma_1 - F_{R1}\right) + \lambda_2^T\left(B_2\Gamma_2 - F_{R2}\right) \tag{6}$$

Equation 6 represents the starting point of derivations in the ground effect and formation analysis. Clearly, some simplification of the governing equations will be desirable. By selecting simpler, characteristic problems, the analysis is more easily performed.

II.A.5. Wake Only Method for Ground Effect

In order to analyze ground effect using the wake only methodology, a real or effective ground plane must be introduced into the model. To do this we exploit the method of images.[30,31] In this analysis, the vortex lattice representing the wake surface is mirrored about the ground or x-y plane(figure 1). In the HallOpt wake only methodology this mirrored wake system is represented as:

$$\Pi = \frac{1}{2}\left(\Gamma_1^T K_{11}\Gamma_1 + \left(\Gamma_1^T K_{1M}\Gamma_M + \Gamma_M^T K_{M1}\Gamma_1\right) + \Gamma_M^T K_{MM}\Gamma_2\right) + \lambda_1^T\left(B_1\Gamma_1 - F_{R1}\right) + \lambda_M^T\left(B_M\Gamma_M - F_{RM}\right). \tag{7}$$

Note, in this case the force constraints are applied to the actual wake (wake 1) and mirrored equivalently to the image wake. In the above equation, the mirrored wake is denoted with an M subscript. By enforcing that the mirrored wake have the identical wake circulation strength,

$$\Pi = \frac{1}{2}\left(\Gamma_1^T K_{11}\Gamma_1 + \left(\Gamma_1^T K_{1M}\Gamma_1 + \Gamma_1^T K_{M1}\Gamma_1\right) + \Gamma_M^T K_{MM}\Gamma_1\right) + \lambda_1^T\left(B_1\Gamma_1 - F_{R1}\right). + \lambda_M^T\left(B_M\Gamma_M - F_{RM}\right). \tag{8}$$

Noting that $K_{M1} = K_{1M}$ and $K_{11} = K_{MM}$, due to the symmetry of the geometry, the power equation can be written as:

$$\Pi = \left(\Gamma_1^T K_{11}\Gamma_1 + \left(\Gamma_1^T K_{1M}\Gamma_1 + \Gamma_1^T K_{M1}\Gamma_1\right) + \Gamma_M^T K_{MM}\Gamma_1\right) + 2\lambda_1^T\left(B_1\Gamma_1 - F_{R1}\right). \tag{9}$$

Taking the variation of equation 9, and making it stationary ($\Pi = 0$), results in the following two equations:

$$\begin{aligned} 2\left(K_{11}\Gamma_1 + K_{1M}\Gamma_1\right) + 2\lambda_1^T B_1 &= 0 \\ 2B_1\Gamma_1 - 2F_{R1} &= 0 \end{aligned} \tag{10}$$

The result, is a simple matrix system (see equation 11) which can be used to determine the minimum power wake circulation distribution as well as the minimum power due to flight near a ground plane (the distance between the flapper and the ground plane is captured by the K_{1M} component of the equation.

$$\begin{bmatrix} K_{11} + K_{1M} & B_1^T \\ B_1 & 0 \end{bmatrix}\begin{bmatrix} \Gamma_1 \\ \lambda_1 \end{bmatrix} = \begin{bmatrix} 0 \\ F_{R_1} \end{bmatrix} \tag{11}$$

Hence, as illustrated in this derivation, the aerodynamic influence of the wake can be directly added to

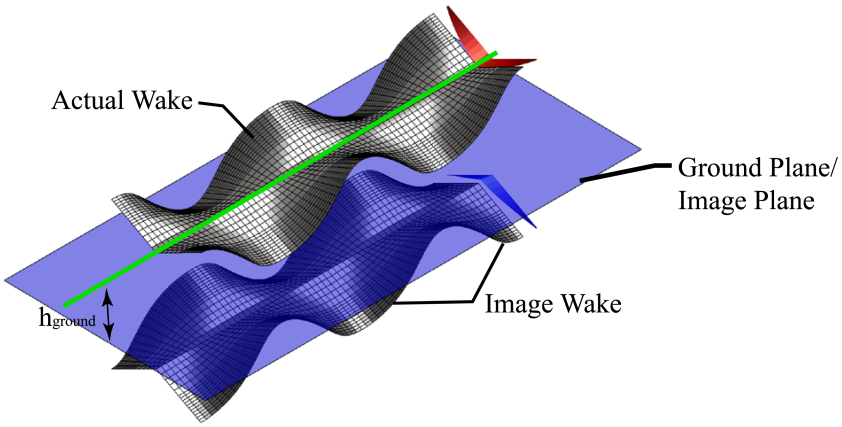

Figure 1. An illustration of the HallOpt real wake and image wake forming an effective ground plane at $y = 0$.

the traditional Hall[50] method in the form of an augmentation of the system matrix to account for the aerodynamics influence from the image wake to the real wake. In addition, we can see from this that the solution of the image wake and real wake circulation distribution is performed simultaneously. Lastly, the

power computation for the two wakes proceeds as usual, except that the power requirement is equally divided between the two wakes. Therefore, the real bird experiences only half of the total power of the system. This distinction is important, but is easily recognized when the simulation considers wakes which have vertical separations of more than 2-3 spans.

II.A.6. Wake Only Method for Formation Flight

Using wake only methods to analyze formation flight requires that simple configurations be considered.[25] Due to the inability to model the near wing aerodynamics, the total power in the wake can be minimized for simple flight considerations. In this paper we consider the simple case of following formation flight. To do this, we define the lead bird to be sufficiently far ahead of the following bird, such that the lead bird is not aerodynamically influenced by the following bird. This allows us to model the lead bird wake as a known, circulation distribution in the flow field. Although this simplification limits the analysis to non-traditional formation flight, this analysis will provide insight into the effects which influence efficient formation flight. In the case of following migratory flight, the lead bird's circulation distribution is prescribed. To determine how

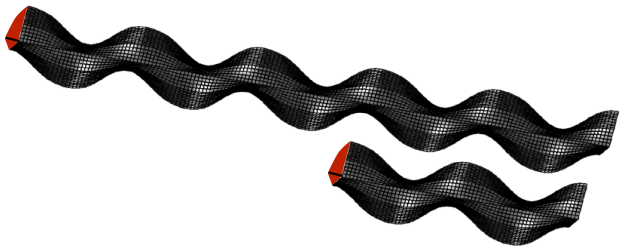

Figure 2. An illustration of the HallOpt wake setup for following migratory flight considerations. The lead bird is so far ahead of the following bird in this case, that the wake can be assumed as a known quantity. This is an ideal situation, but, provides insight into the flapping kinematics required for optimal energy extraction strategies.

the following bird formation flight situation is performed in the HallOpt framework, we once again derive the linear system for this special case (starting from equation 6):

$$\Pi = \frac{1}{2}\left(\Gamma_1^T K_{11}\Gamma_1 + \left(\Gamma_1^T K_{1L}\Gamma_L + \Gamma_L^T K_{L1}\Gamma_1\right) + \Gamma_L^T K_{LL}\Gamma_2\right) + \lambda_1^T\left(B_1\Gamma_1 - F_{R1}\right). + \lambda_L^T\left(B_L\Gamma_L - F_{RL}\right). \quad (12)$$

In this case the wake of the lead bird is denoted using the subscript L. The variation of equation 13 can be taken and set to zero. Note, that the variation of the lead bird wake variables is zero (since it is prescribed). This results in the following two equations:

$$\begin{array}{cc} \left(K_{11}\Gamma_1 + \frac{1}{2}\left(K_{1L}\Gamma_L + K_{L1}^T\Gamma_L\right)\right) + \lambda_1^T B_1 & = 0 \\ B_1\Gamma_1 - F_{R1} & = 0. \end{array} \quad (13)$$

The result is the linear system solution presented in equation 14

$$\begin{bmatrix} K_{11} & B_1^T \\ B_1 & 0 \end{bmatrix}\begin{bmatrix} \Gamma_1 \\ \lambda_1 \end{bmatrix} = \begin{bmatrix} -\frac{1}{2}\left(K_{1L}\Gamma_L + K_{L1}^T\Gamma_L\right) \\ F_{R1} \end{bmatrix} \quad (14)$$

The resulting linear system which is solved is similar to the single flapping wing case, with the only difference occurring in the RHS of the linear system. In effect, the augmentation which is performed in the RHS of the linear system acts as a drag, equivalent to what is seen in the viscous augmentations of the method by Hall et al.[50] It is clear that the wake only analysis here for formation flight is an idealization, and as such, is considered useful for predicting formation trends. Additionally, due to the manner in which the wake vorticity minimum power problem is solved, we can only expect that the results of the analysis to be trend accurate and not quantitatively to be trusted.

II.A.7. Analysis Assumptions

The following assumptions are made in the wake only analysis of ground effect and formation flight of flapping wing vehicles.

- In this analysis we assume that the effects of viscosity on the wake diffusion are minimal. This is likely a valid assumption for most instances of energy saving flight.
- In the analysis we assume the induced effects on the first order forces to also be negligible. This assumption is likely to be invalid when wings and ground planes are in close proximity to each other.
- Although the effects of dissipation and diffusion are assumed negligible in the determination of optimal positioning and flapping frequency, we assume flapping phase and flight location are important.
- We assume that the wake shapes are rigid and do not have inter-wake influences. Although the shape of the wake is likely to be un-representative of the complex vortex-vortex interactions taking place, this assumption is assumed to have only a small effect.

III. Flapping Geometry Description

In this paper we consider simple harmonic flapping about a central hinge to define the wake geometry. The wake geometry is represented as:

$$X(t) = t; \tag{15}$$

$$Y(t) = W\cos(\omega t) \tag{16}$$

$$Z(t) = W\sin(\omega t) \tag{17}$$

In this paper we consider flapping wings which produce a single lift coefficient ($C_L = 0.1 = \frac{L}{\frac{1}{2}\rho U^2 b^2}$ as used by Hall et al.[50]). Several thrust coefficients are examined ($C_T = 0.0025$, $C_T = 0.005$, $C_T = 0.01$, $C_T = 0.02$, and $C_T = 0.04$, where $C_T = \frac{T}{\frac{1}{2}\rho U^2 b^2}$). For each of these thrust to lift ratios, a baseline frequency-amplitude parameter sweep was performed in addition to the formation flight and ground effect analysis.

IV. Parameter Sweep Experiments : Baseline Experiments

Several reference baseline experiments are performed in two- and three-dimensions to allow comparison with the results from the analysis. The baseline parameter sweeps are primarily concerned with describing the regions of low power flight (or highly efficient flight) with flapping amplitude and frequency as variables. The baseline cases for all of the experiments performed in this paper refer to a single flapping vehicle isolated from the ground as well as from any domain vorticity influence. The induced and total power for achieving flight by flapping are recorded in table 1. The baseline parameter sweeps are pictorially shown in fig.11.

Table 1 shows the optimal power coefficient values determined from the baseline investigations.

Table 1. The minimum values for total and induced power for different lift and thrust constraints

F.O.Lift*	F.O.Thrust*	Total Power	Inviscid Power	P_I/P_T
0.1	0.0000	0.0046	0.0031	0.667
0.1	0.0025	0.0050	0.0034	0.673
0.1	0.0050	0.0054	0.0036	0.674
0.1	0.0100	0.0064	0.0042	0.671
0.1	0.0200	0.0082	0.0055	0.668
0.1	0.0400	0.0125	0.0086	0.693

* The lift and thrust values listed here are first order lift and thrust values.[50]

V. Parameter Sweep Experiments : Ground Effect

In order to investigate the ground plane effect on energy savings in lift and thrust producing flapping wings, several parameter sweeps were undertaken. The aim of this study was to evaluate the effects of increasing the thrust requirements. The goal was to determine from these trends what benefits or negative aspects there are to flapping near the ground plane while producing lift and thrust simultaneously on a

single surface. The detailed results for parameter sweeps for a single flapper at various distances from the ground plane are shown in figures 13 -22. These computations are identical to the baseline flapping flight parameter space design sweeps except for the introduction of the mirror image of the wake to setup the appropriate ground plane. In addition to the design space sweeps, the minimum power coefficient, for the valid portion of the design space, is recorded and plotted for each configuration of prescribed lift and thrust. The minimum power of the design space sweep is plotted with respect to the height above the ground plane. The pictorial representation of the kinematics of the two ground effect design sweeps are shown in figure 3. In this analysis, two separate flapping strategies were considered. One with a mean flapping angle

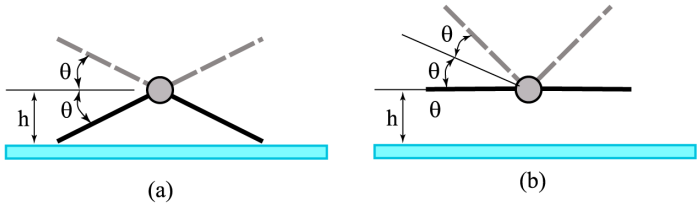

Figure 3. A pictorial representation of the flapping in the ground effect case. In (a) the symmetric flapping is represented (as seen from infront of the bird). In (b) the forced positive dihedral scenario is illustrated (again, as seen from infront of the bird). Note, that for the same flapping angles (θ), and elevation h the bird has a different tip clearances with the ground plane. Thee two extreme cases were examined to determine if either was beneficial.

corresponding to the horizontal plane (figure 3a.) and another configuration where the minimum flapping angle correspoded to the horizontal plane (figure 3b).

V.A. Summary of Results and Discussion of Ground Effect In Flapping

Figures 4 and 5 illustrate the normalized best-case savings due to ground effect at different heights above the ground plane for different thrust coefficient requirements. The parameter sweeps from which these results were extracted can be seen in in figures 13-22. It is clear from these results that the vertical distance of the wing from the ground plane is of paramount importance in both flapping and rigid wing flight. In flapping flight when thrust requirements are increased, efficient generation of this thrust occurs when the wings flap with greater amplitude. As such, as the thrust requirement from the wings increases, we expect the effects of higher amplitude flapping to be seen in the ground effect results (with the strict limitation that the flapping amplitude does not allow the wings to hit the ground plane). In figure 4 the results are shown for simple symmetric flapping case ((see figure 3a)where the maximum angular amplitude of flapping is the same in both upwards and downwards direction from the body) . In this case, when the bird is close to the ground, the optimal savings occur when the wings flap and nearly touch the ground plane on the maximum extent of the downstroke. In the results illustrated in figure 5 the wings are flapped such that the maximum downwards amplitude of flapping lies in the same horizontal plane as the body (see figure 3b). In this case, the wings are always observed with positive dihedral. In figures 4 and 5, the results of the ground effect study are plotted and compared with the results from several ground effect approximations[46–48] for rigid wings as presented by Rayner.[27] The results which are reported in each of the other experiments show induced drag savings only (the normalization of the drag savings is with respect to the induced drag and not the total drag). As such, we plot the normalized induced drag savings component (blue) as well as the normalized total drag savings (black) for the different flappers at different heights above the ground. It can be seen from these results that the induced drag savings for low amplitude flappers ($C_T = 0.0025$) compare well with the results of the other references. Some differences can be observed in the cases.

1. For the positive dihedral flight case, the drag savings are observed to degrade with increased thrust requirement. This is expected, since, the height of the wings is on average further away from the ground plane than in the symmetric flapping analysis. This result implies that, in ground effect flight, the flapping kinematics should be tuned, such that the desired amplitude of flapping is achieved with the wingtips as close to the ground as possible during the downstroke (this way the flapping wing gains more energy savings from the ground plane effect on average through the flapping cycle). This requirement will be investigated in future design space sweeps and studies of this phenomena.

2. For the symmetric flapping wing in ground effect, the savings appear to be greater than those observed

in the other references. One reason for this is that we consider optimal vorticity distributions in this study. In addition, it is possible that the downstroke (which has a downwards orientation to the body which is at the reference height) allows the bird to exploit more energy savings from the ground plane effect at lower altitude flights (Since the wing reaches a position closer to the ground). This is a preliminary result which will be further investigated.

3. Considering the results which include viscous effects in the approximation of drag savings illustrates that the cases with increased thrust requirement have less potential for savings than the lower thrust cases. This is primarily due to the increased viscous load on these birds due to the increased thrust requirement. The viscous loads, although slightly altered by the ground effect (due to finer details of the flow and the adjustment of the circulation distribution), do not experience similar savings potential as the induced drag. Hence, the overall normalized savings in higher amplitude flapping is less than in lower amplitude flapping, despite the potential for increased induced savings.

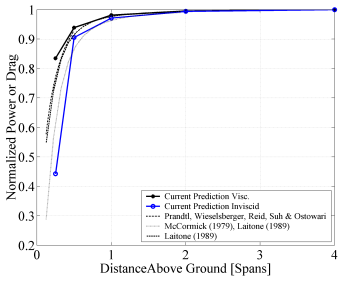

(a) $C_T = 0.0025$, Symmetric Flapping Case

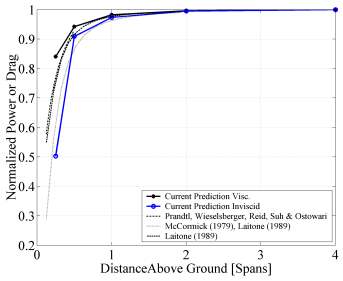

(b) $C_T = 0.005$, Symmetric Flapping Case

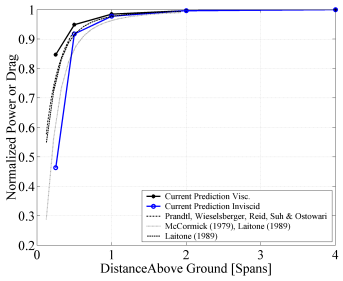

(c) $C_T = 0.01$, Symmetric Flapping Case

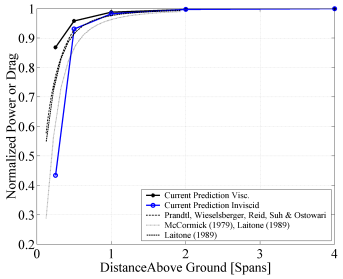

(d) $C_T = 0.02$, Symmetric Flapping Case

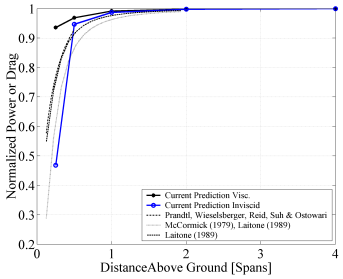

(e) $C_T = 0.04$, Symmetric Flapping Case

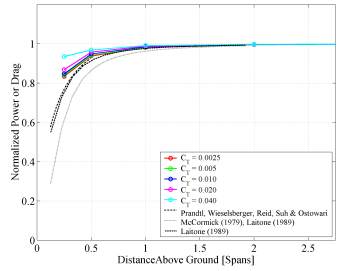

(f) The illustration of the total power reduction as a function of height above the ground overlaid for all thrust requirements.

Figure 4. A summary of the experiments for the ground effect case when the wings beat in up-down symmetry about the body axis (see figure 3a). The plots illustrate the current prediction for ground effect savings as compared with Prandtl-Weiselsberger-Reid Theory,[46] McCormick-Laitone Approaches[47] and Laitone modified approximations,[48] as presented in Rayner.[27] Note that, from Rayner,[27] the models should all match in the above range. As expected, agreement is observed for the low amplitude flapping ($C_T = 0.0025$), induced drag or inviscid computations using the current method.

In conclusion, it is likely that, in the optimal ground effect kinematics, the downstroke always has a minimum up-down flapping angle corresponding with the wing tip touching or nearly touching the ground surface. This would likely maximize the savings in the downstroke, while making the average wing position as close to the ground as possible during flapping. This effect is noticed in the detailed design space sweeps for the cases examined in this paper (see figures 13-17, and notice the cases where the ground proximity limits the design space side). In most of the symmetric flapping cases (see figure 3a, and figures 13-17), the minimum power for the cases near the ground is found to be on the limiting line representing the wingtip hitting the ground plane surface. In future examinations of ground effect using these methods, the wing tip proximity to the

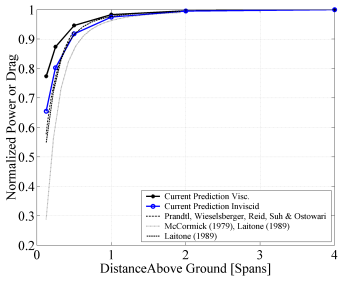

(a) $C_T = 0.0025$, Positive Dihedral Case

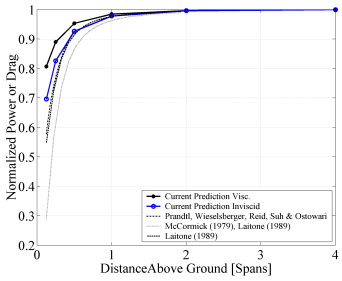

(b) $C_T = 0.005$, Positive Dihedral Case

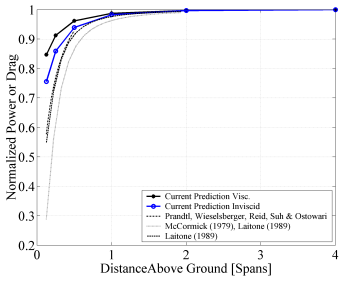

(c) $C_T = 0.01$, Positive Dihedral Case

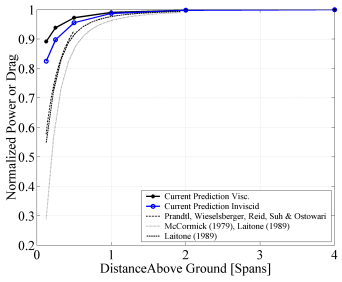

(d) $C_T = 0.02$, Positive Dihedral Case

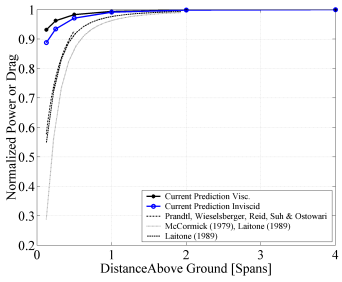

(e) $C_T = 0.04$, Positive Dihedral Case

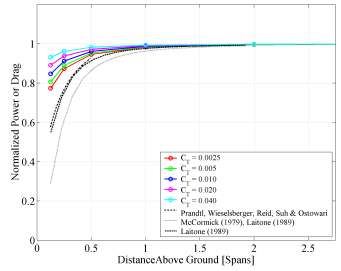

(f) The illustration of the total power reduction as a function of height above the ground overlaid for all thrust requirements.

Figure 5. A summary of the experiments for the ground effect case when the wings beat with positive dihedral at all points in the flapping cycle (see figure 3b). The plots illustrate the current prediction for ground effect savings as compared with Prandtl-Weiselsberger-Reid,[46] McCormick-Laitone[47] and Laitone,[48] as presented in Rayner.[27] Note that, from Rayner,[27] the models should all match in the above range. This agreement is observed for the low amplitude flapping ($C_T = 0.0025$), induced drag or inviscid computations using the current method. It can also be seen, that as the thrust requirement increases, the current method predicts less savings (likely a by-product of the restriction that wings have positive dihedral throughout the flapping cycle) .

ground will be fixed and the wings will be allowed to flap upwards to any extent desired. This would more appropriately mimic the limitations in nature and also provide a more detailed view of the limiting factors and the kinematics modifications required in flapping flight.

VI. Formation Flight Results

In the formation flight case, the relative position between the lead bird and the following bird is examined. As is observed in nature and in formation flight of aircraft, the beneficial energy-saving region of interest is outboard of the wingtips of the leading lift producing vehicle (this is where the lead vehicle upwash is found). We expect the case to be similar for flapping flight; however, additional considerations may place stricter requirements on the position and wing-beat phase of the following vehicle with respect to the leading vehicle if optimal power reduction is to occur. For example, the non-uniform wake circulation shed by the lead bird will have regions of greater upwash during the downstroke (in particular at mid downstroke) and as such, it is likely that the following bird would benefit from flapping into that upwash. Additionally, considerations such as the wingtip vertical position of the following bird with respect to the wing tip trace of the lead bird may prove to be important (we assume in this experiment that the wakes do not roll-up due to self influence, and as such, the spatial location of circulation remains fixed once it has been shed from the wing). The following bird should capture as much upwash as possible, and it is likely that there is a phase and an $y-z$-plane location of the midline of the bird at which these induced power savings are achieved optimally.

To reduce the computational design space to a tractable one while maintaining a level of consistency, the wake shape of the lead bird and the following bird are set to be identical (we assume both birds have identical flapping motions). The two birds are also required to produce the same lift and thrust per cycle (with no net average sideforce or net average roll-moment). Not only are the wakes identical, but the actual shape of the wakes are the optimal ones determined from the baseline flapping flight design space sweeps (see figure 12). By prescribing the lead and following bird to have the same wake geometry (frequency and amplitude), the only unknown which remains in the formation flight is the position of one wake relative to the other. In order to define the relative positions of one wake to another, the lead bird is defined to lie on the x-axis (flying in the positive x-direction, with the top of the upstroke occurring at $x = 0$). The mid-line or flight path of the following bird is defined by the y- and z- offsets from the lead bird. This means, that the following bird's $y - z$ position is indicative of the body position (with respect to the body position of the lead bird). The x-position of the following bird defines the position of the body at which the top of the maximum vertical excursion of the wing occurs during flapping (relative to the lead bird, whose maximum vertical wing position commences at $x = 0$). Therefore, if the x-position is zero, the wings are in phase, it the x-position is $\frac{1}{2}$ of the wake length, then the wings are π-radians out of phase(see figure 6). Although we state that the wings are out of phase, the visual flapping may or may not be out of phase depending on the physical streamwise position offset. Here, we are interested only in the geometrical location of the wake and not the time history of the wake development (ie. two birds may beat their wings out of phase, but upon closer inspection, the trailing bird may be flying geometrically in phase with the lead bird, by following it's physical shed wake, and not matching the motion of the lead bird's wings).

Computations of power for birds with different $y-z$-positions are performed for sixteen intervals along a wake period ($x - direction$) to determine the optimal physical space phase shift between the flapping wings. These sixteen intervals are denoted $s0 - s16$ as illustrated in figure 6 . In addition, the y-location (spanwise) of the following bird is examined for a range which has no spanwise separation at the low end (one bird on top of the other) to $y = 1.5$ spans (the birds' wingtips are separated by half a span of distance in y). In the vertical direction, the wakes are arranged such that the scan occurs from one span above the lead bird, to one span below the lead bird. At each point in the cube-shaped design space, the induced power required by the following bird's flight is computed. The power is then plotted for each relative position of the birds in figures 24-28. It should be noted that the plots do not necessarily indicate regions of preferred flight, but rather regions in which the body of the following bird should be located **when** it starts its flapping cycle (spatial phase considerations). In other words, the contour plots show the required flight power for a particular spacing at the location where the center of the wing lies when the flapping motion starts.

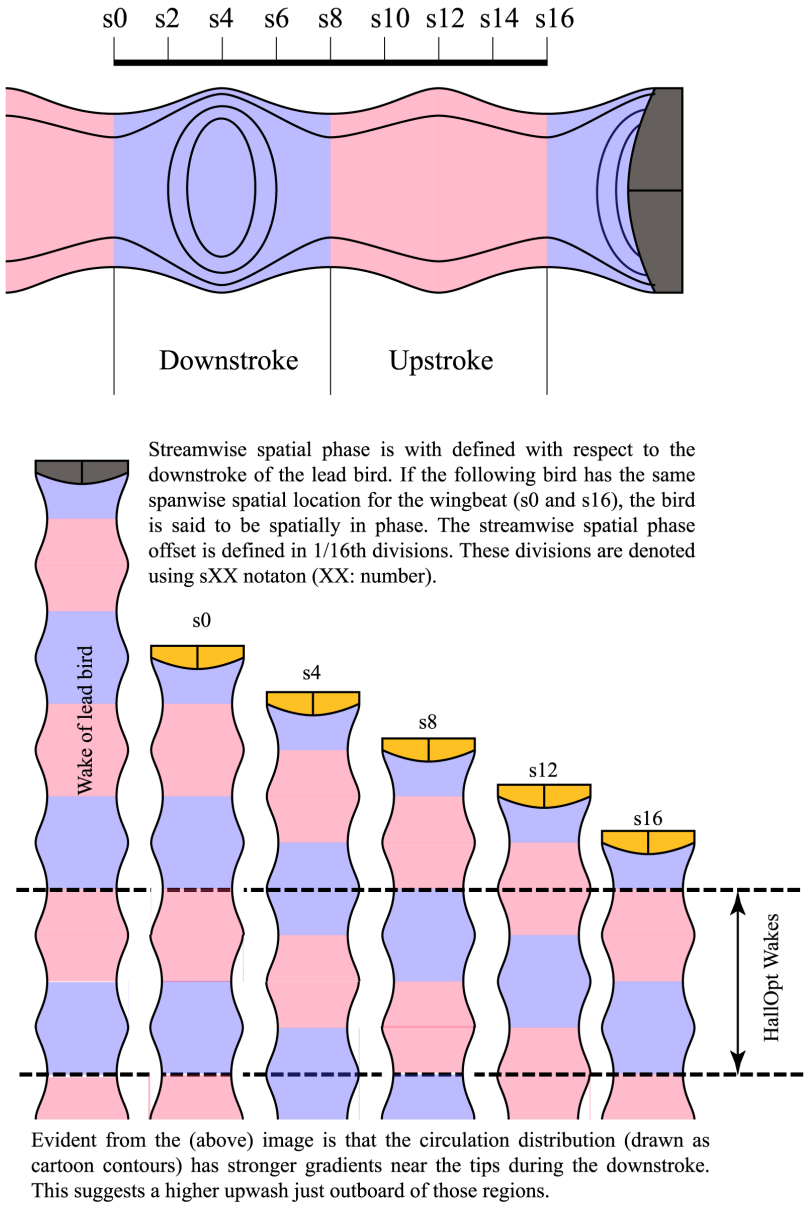

Figure 6. A pictorial representation of the formation flight configuration for the case examined in this paper. Although many wakes are presented in the figure, we only examine a single lead bird and following bird wake at a time (2 wakes total).

VI.A. Discussion of Formation Flight with Flapping

The flapping formation flight scenario exhibits energy savings when the following bird is outboard of the lead bird with a very slight overlap of the wings. It was found in order to achieve the most energy savings in formation flight, that the following bird should beat its wings spatially in phase with the lead bird. This requirement is conceptually simple, since, in order to benefit the most from the upwash of the lead bird's downstroke, the following bird must stroke downwards at that same spatial location. Figure 7 summarizes the results (which are in included in pictorial form in the appendix for completeness). The results in figure

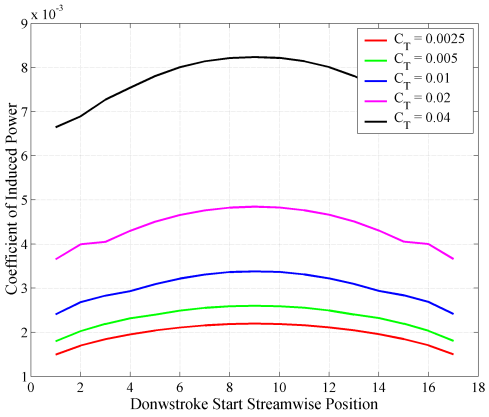

(a) A plot showing the induced coefficient of power for the following bird due to formation flight. note the lead bird does not receive any savings due to the assumption that it is far ahead of the following bird. This plot is concerned with the region in which **no** wingtip overlap occurs (to minimize the potential for vortex lattice related anomalies if they exist). Hence, all birds in this plot have an *inter-body separation of at least one wingspan.*

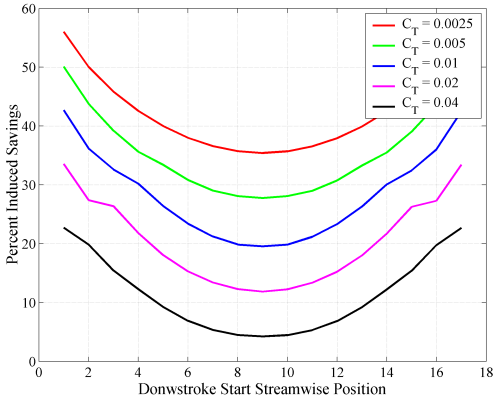

(b) The percent total power savings due to formation flight. This plot is concerned with the region in which **no** wingtip overlap occurs (to minimize the potential for vortex lattice related anomalies if they exist). Hence, all birds in this plot have an inter-body separation of at least one wingspan.

Figure 7. A summary of the runs for the formation flight case. In this example the minimum achievable power coefficient for different x-wise locations of the start of downstroke is shown (where the lead bird starts its downstroke at $x = 0$ and finished the upstroke at $x = 16$. What this result clearly displays is that, the following bird should start its downstroke near the spatial position of the start of the downstroke of the leading bird.

7 illustrate that the flight of the following bird is most effective if its wings flap in the same spatial locations as the lead bird (spatially in phase). The results suggest that upwards of twenty percent variation exists in the induced flight power savings if flapping is done optimally in phase vs. sub-optimally out of phase. Although, precision phase locking is not required for energy savings to occur (flying anywhere outboard of the tips of the lead bird yields some form of savings) it is an avenue worthy of exploration if a bird wishes to minimize its power as much as possible. Figure 8 is a representative contour slice of the following bird's power expenditure as a function of position of the start of downstroke. As can be seen from this representative image, the wing is best served to beat in spatial phase with the lead bird wake. It appears from figures 7-8, that the savings for formation flight are maximized when the lead and following bird are in spatial phase. This condition of spatial phase locking appears to provide significant savings over the π-radians out of phase scenario. Although, precise phase-locking provides the ultimate energy savings, near-phase locking also provides significant reductions in power. The aim of the phase locking is two fold, first, to track and capture the lead bird's vortex wake most effectively, the following bird must be spatially near the tip vortex, and second, the maximum upwash is located outboard of the position at which the lead bird performed a downstroke. This means that the following bird should ideally perform its downstroke at the same position.

The final consideration in the formation flight problem is the relative vertical position of the following bird's body with respect to the lead bird's wing . The condensed illustration in figure 10 shows that ideally the following bird would not be vertically elevated above or below the lead bird wake (if flapping started in phase as would be desired). If however, the following bird is not flapping in phase with the lead bird, the figure shows that it may be advantageous to take on a vertical displacement relative to the lead bird to most

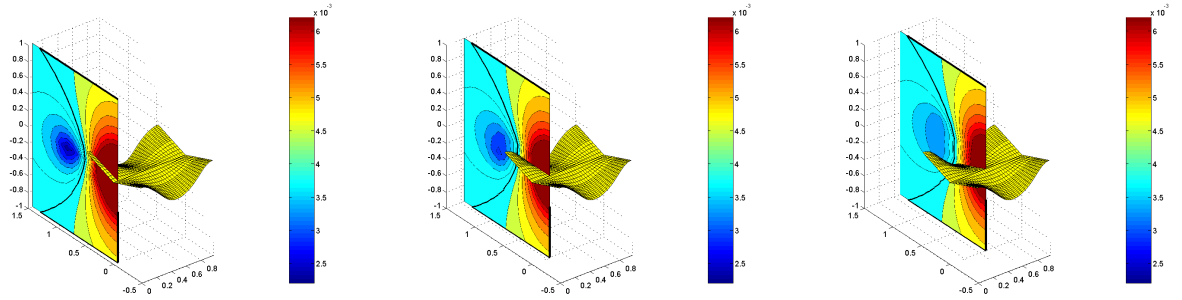

(a) $C_T = 0.01$, Following bird in phase with the lead bird

(b) $C_T = 0.01$, Following Bird out of phase by $\frac{\pi}{2}$ from the lead bird

(c) $C_T = 0.01$, following bird out of phase by π from the lead bird flapping

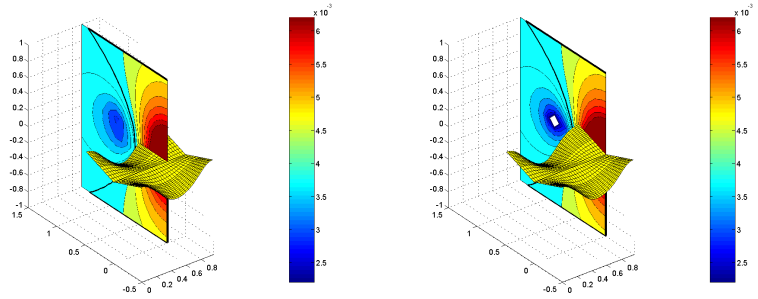

(d) $C_T = 0.01$, following bird out of phase by $-\frac{\pi}{2}$ from the lead bird

(e) $C_T = 0.01$, following bird in phase with the lead bird

Figure 8. Power coefficient contour slices for $C_T = 0.01$, $C_L = 0.1$, representing where the energy saving zones for flapping are located. In these plots, a region of low power represents the position of the mid-line of the body, when the bird starts its flapping cycle. At this stage in the analysis, it is possible to see a preference for the flapping motions of the following bird which mimic the lead bird (in space). This can be seen from the clustering of the lower power values near the start and end of the wake period. The bold contour on each of the plot separates flight positions which achieve power savings from those that do not.

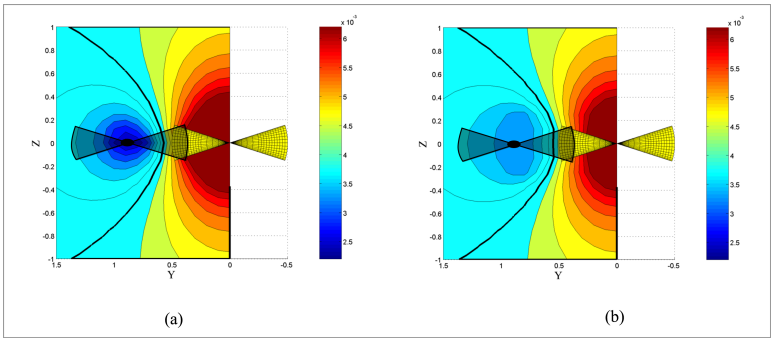

Figure 9. An illustration of the power coefficient contour plots for the same case as shown in figure 8 but shown for the (a) best and (b) worst cases of steamwise phase shift (in (a) the following bird beats with the same up-down positions as the lead bird; however, in (b) the spatial flapping phase shift is π-radians – meaning, the spatial location in which the lead bird had a downstroke, the following bird performs an upstroke, and visa-versa) . In this figure we have overlaid the position of the following bird (in transparent black/grey) to illustrate the most effective $y - z$ spacing. Outboard of the bold contour, positive savings are realized.

effectively capture the lead birds strongest upwash regions. It is likely that these vertical displacements do not happen in nature for aerodynamic benefit due to the fact that precision flight dynamics and sensing would be required.

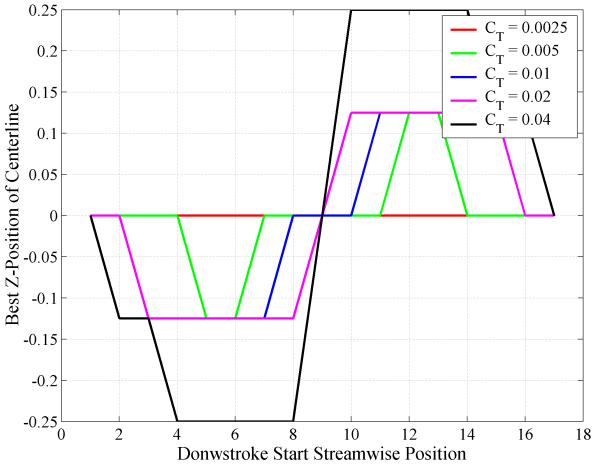

Figure 10. The optimal vertical position of the body or centerline of the wing, for different phase shifts between the lead and the following bird. The lead bird starts at the top of the upstroke initially ($x = 0$) and returns to that position at $x = 16$.

In this analysis of flapping formation flight we observe significant benefits relating to phase locking of the flight of the lead and following bird. This physical space phase locking is intuitive, as the following bird would be able to effectively capture the vorticity of the lead bird throughout the extent of the wingbeat cycle. Although there are varied reports of wingbeat phase locking in natural formation flight we predict in this paper that it would be beneficial to lock the spatial phase of the wingbeat (this would require knowing the location of the vorticity in the fluid which the following bird exploits). This suggests that the lead bird and following bird would exhibit similar freuency and amplitude of flapping. In order to achieve this spatial phase locking requirement, it is likely that some form of visual cue would be required (similar to walking in the footprints left by another person, the following bird may need to observe the kinematics of the lead bird). As such, **if**there is indeed a spatial phase locking in natural formation flight, it is possible that the shape of the formation is such that this locking can be done using visual cues. Although there is much uncertainty of whether phase locking occurs in nature, this hypothesis may confirm both the aerodynamic savings and the behavioral advantage of formations. If, however, spatial phase locking is not exploited in nature (due to the difficulties involved), it is likely that, on average, the following bird will periodically garner the advantages of similar phase flapping motions, and therefore achieve acceptable savings. Finally, non-optimal formations may be observed in nature (larger spanwise wingtip spacings, no phase locking etc.) due to other considerations such as stability and control, and unpredictable votex-wing interactions.

VII. Future Directions

What has been presented in this paper is a preliminary examination of the potential benefits of flapping in ground effect and formation flight. Subsequent investigations are planned to focus more closely on the results of this study. These investigations will expand on the current study while also exploiting the ongoing research into multiple fidelity level tools[62] for flapping flight. As such, some of the limiting assumptions and simplifications in this analysis may be addressed, and a more reliable picture of the energy savings can be formed.

VIII. Conclusions

In this paper a preliminary numerical investigation of ground effect and migration has been performed. In the case of ground effect, we observe that wings with a closer average position to the ground plane will have greater energy savings. In addition, from the symmetric and positive-dihedral-only ground effect cases,

we postulate that wingbeat kinematics near a ground plane surface may gain advantage by being adjusted so that the maximum downwards excursion of wing corresponds to the wingtip nearly touching the ground plane, while the upward excursion of the wing is only limited by the maximum angle of $\frac{\pi}{2}$ radians (to prevent wing cross-over). This *tip nearly touching* scenario will be the subject of future investigations. In the case of formation flight, we found that wake spatial phase locking between the lead bird and following bird is advantagous. This allows the following bird's wing tip to be closer to the vorticity shed by the lead bird at all points in the flapping cycle, while also allowing the following bird to exploit the maximum upwash (from the lead bird's downstroke) during its own downstroke.

The results are from a preliminary investigation using wake only methods, and as such need to be confirmed with higher-fidelity tools. In addition to confirming many of the results presented in this paper, higher fidelity methods with good initial starting points may also be able to shed more light onto the formation configuration which is optimal for flapping wings. In formation flight, it is possible, that, with the increased vorticity shedding during the downstroke, that streamwise stagger is less critical than the spatial phase locking of the wake capture process.

Acknowledgments

This material is based upon work supported by the National Science Foundation under Grant No. 0540266 and 0540203.

References

[1]J.M.V. Rayner, *Fat and formation in flight*, Nature, Vol. 413, pp 685-686, 2001.

[2]Gill, F.B., *Ornithology, 2nd Edition*, W.H.Freeman and Company, New York, 1994.

[3]Alexander, R.M., *Exploring Biomechanics. New York: Scientific American Library, 1992.*

[4]J.T. Emlen, Flocking behavior in birds, *Auk, vol. 69, pp. 160-170, 1952.*

[5]Badgerow, J. P., An analysis of function in the formation flight of Canada Geese., *Auk 105: 749-755, 1988.*

[6]Badgerow, J.P., and Hainsworth, F.R., Energy savings through formation flight? A reexamination of the Vee formation. *J. Theor. Biol. 93: 41-52., 1981.*

[7]Weimerskirch, H. et al., *Proc. R. Soc. Lond. B 267,1869-1874 (2000).*

[8]Hainsworth, F. R., Induced Drag Savings From Ground Effect and Formation Flight in Brown Pelicans, *J. Exp. Biol. 135, 431-444 (1988).*

[9]Hainsworth, F. R.,Precision and Dynamics of Positioning by Canada Geese Fying in Formation, *J. Exp. Biol. 135, 431-444 (1988).*

[10]Cutts, C, Speakman, J, Energy Savings in Formation Flight Of Pink-Footed Geese, *J Exp Biol 1994 189: 251-261*

[11]T.C. Williams, T.J. Klonowski, and P. Berkeley, Angle of canada goose flight formation measured by radar, *Auk, vol. 93, pp. 554-559, July 1976.*

[12]N.O'Farell, J. Davenport, and Thomas Kelly, Was *Archaeopteryx* a wing-in-ground effect flier?, *Ibis, Vol 144, pp 686-688, 2002.*

[13]Blake, R. W., Mechanics of gliding in birds with special reference to the influence of ground effect. *.I. Biomech. 16,649-654, 1983.*

[14]Blake, R. W., A model of foraging efficiency and daily energy budget in the black skimmer (Rhynchop.c nigra). *Can.J. Zool. 63, 42-48, 1985.*

[15]Withers, P. C., Aerodynamics and hydrodynamics of the 'hovering' flight of Wilson's storm petrel. *J. exp. Hiol. 80, 83-91, 1979.*

[16]Withers, P. C. and Timko, P. L., The significance of ground effect to the aerodynamic cost of flight and energetics of the black skimmer (Rhynchops nigra). *J. exp. Biol. 70, 13-26, 1977.*

[17]F. R. Hainsworth, Induced Drag Savings from Ground Effect and Formation Flight in Brown Pelicans, *J. exp. Biol., vol 135, pp. 431-444, 1998.*

[18]Norberg, U. M. and Rayner, J. M. V., Ecological morphology and flight in bats (Mammalia; Chiroptera) : wing adaptations, flight performance, foraging strategy and echolocation. *Phil. Trans. R. Soc. Lond. B 316, 335-427, 1987.*

[19]F.H. Heppner, Avian flight formation, *Bird Banding, vol. 45, no. 2, pp. 160-169, 1974.*

[20]Heppner, F.H., Convissar, J.L., Moonan jr., D.E., and Anderson, J. G.T., Visual Angle and Formation Flight in Canada Geese (Branta canadensis), *Auk Vol. 102, 1984.*

[21]Malte Andersson , and Johan Wallander, Kin selection and reciprocity in flight formation *Behav. Ecol. 15: 158-162.*

[22]Y.Moryoseff and Y.Levy, Computational study of the Flow about an Oscillating Wing in Ground Effect, *AIAA 2001-0863, Reno, NV, 2001.*

[23]Lissaman, P. B. S. and Shollenberg, C. A., Formation Flight of Birds, *Science 168, 1003?1005 (1970).*

[24]P. Lissaman, Simplified Analytical Methods for Formation Flight and Ground Effect, *AIAA Paper 2005-851, Reno, NA, 2005.*

[25]R.M.King and A. Gopalarathnam, Ideal Aerodynamics of Ground-Effect and Formation Flight, *AIAA 2004-906, Reno, NV, 2004.*

[26]Widnall, S. E. and Burrows, I. M., An analytical solution for two- and three-dimensional wings in ground effect. *J.Fluid Mech. 41, 769-792, 1970.*

[27]J.M.V. Rayner, On the Aerodynamics of Animal Flight in Ground Effect, *Phil. Trans.: Bio. Sciences, Vol. 334, No. 1269, pp: 118-128, 1991.*

[28]W. Cole, The PelicanL A big bird for the long haul, *Boeing Frontiers Online, Vol. 01, Issue 5, 2002.*

[29]M. Halloran and S.O'Meara, Wing in Ground Effect Craft Review, *DSTO Aeronautical and Maritime Research Laboratory, Melbourne, Australia, 1999.*

[30]H.Lamb, Hydrodynamics, *Dover Publications, 6th Ed., 1993.*

[31]O.D.Kellogg, Foundations of Potential Theory, *Springer, 1967.*

[32]C. Han and W. H. Mason, Inviscid Wing-Tip Vortex Behavior Behind Wings in Close Formation Flight, *Journal of Aircraft 2005-0021-8669 vol.42 no.3 (787-788), 2005.*

[33]William B. Blake and David R. Gingras, Comparison of predicted and measured formation flight interference effects, *AIAA-2001-4136, AIAA Atmospheric Flight Mechanics Conference and Exhibit, Montreal, Canada, Aug. 6-9, 2001*

[34]K. Jones and M. Platzer, Bio-Inspired Design of Flapping-Wing Micro Air Vehicles - An Engineer's Perspective, *AIAA-2006-37, Reno, NV., 2006.*

[35]G.A.Dimock and M.S. Selig, The aerodynamic benefits of self-organization in bird flocks, *AIAA Paper 2003-608, Reno, NV, 2003.*

[36]S. Iglesias and W.H.Mason, Optimum Spanloads in Formation Flight, *AIAA Paper 2002-1358, Reno, NV., 2002.*

[37]M.S. Triantafyllou, G.S.Triantafyllou, and D.K.P.Yue,Hydrodynamics of Fishlike Swimming, *Ann. Rev. of Fluid Mechanics, 32: 33-53, 2000.*

[38]F.E. Fish, and G.V. Lauder, *Passive and Active Flow Control by Swimming Fishes and Mammals, Ann. Rev. of Fluid. Mech., vol 38: 139-224, 2006.*

[39]May, R.M., Flight Formations in Geese and Other Birds, *Nature 282, 778 - 780 (20 Dec 1979) News and Views.*

[40]C.J.Cutts and J.R.Speakman, Energy Savings in Formation Flight of Pink-Footed Geese, *J. exp. biol., Vol 189, pp. 251-261, 1994.*

[41]Z.A. Bangash, R.P.Sanchez, A. Ahmed, and M.J.Khan, Aerodynamics of formation flight, *AIAA Paper 2004-725, Reno N.V. 2004.*

[42]M. Munk, The Minimum Induced Drag of Aerofoils, *Report No. 121.*

[43]G.V.Schweppenberg,Vorteile der Zuggeselligkeit *Vofelwarte 16, 116-119, 1952.*

[44]Nachtigall, W., Phasenbeziehungen der Flugelschlage von Gasen wahrend des Verbandflugs in Keilformation, *Z. vergl. Physiol., vol 67. 414-422, 1970.*

[45]M. Berger, Formationsflug ohne Phasenbeziehung der Flugelschlage, *Journal of Ornithologym Vol. 113, no. 2, 1972.*

[46]Y.B. Suh and C. Ostowari,*Drag reduction factor due to ground effect J. Aircraft, 25, 1071-1072, 1998.*

[47]B.W.McCormick, Aerodynamics, aeronautics and flight mechanics, *New York : John Wiley, 1979.*

[48], E. V. Laitone, Comment on 'Drag reduction factor due to ground effect, *J.Aircraft 27, pp. 96, 1989.*

[49]Hall, K. C., and Hall, S. R., Minimum induced power requirements for flapping flight *Journal of Fluid Mechanics, 1996, Vol. 323, pp. 285-315.*

[50]Hall, K. C., Pigott, S. A., and Hall, S. R., Power Requirements for Large-Amplitude Flapping Flight *Journal of Aircraft, Vol. 35, No. 3, 1998, pp. 352-361.*

[51]Hall, K. C., and Pigott, S.A., Power Requirements for Large-Amplitude Flapping Flight, *AIAA Paper 97-0827, Presented at the 35th Aerospace Sciences Meeting and Exhibit, Reno, NV, Jan. 6-9, 1997.*

[52]D.J. Willis, J.Peraire, M.Drela, and J.K.White, A numerical Exploration of Parameter Dependence in Power Optimal Flapping Flight, *AIAA-2006-2994, An Francisco, 2006.*

[53]D.J.Willis, J.Peraire and J.K.White, A Combined pFFT-multipole tree code, unsteady panel method with vortex particle wakes, *Int. J. Numer. Meth. Fluids, 53, 1399-1422, 2007.*

[54]X. Tian, J.Iriarte, K. Middleton, R.Galcao, E.Israeli, A. Roemer, A.Sullivan, A.Song, S. Swartz, K.Breuer Direct Measurements of the Kinematics and Dynamics of Bat Flight, *Bioinspiration and Biommimetics, 1:S10-S18.*

[55]A.Hedenstrom, L.C. Johansson, M.Wolf, R.von Busse, Y.Winter, and G.R.Spedding, Bat Flight Generates Complex Aerodynamic Tracks, *Science, Vol. 316, no. 5825, pp 894-897, 2007.*

[56]G.R.Spedding, M.Rosen, and A.Hedenstrom, A family of vortex wakes generated by a thrush nightingale in free flight in a wind tunnel over its entire natural range of speeds, *J. Exp. Biol., 206, pp 2313-2344, 2003.*

[57]I. Kroo, Drag Due to Lift: Concepts for Prediction and Reduction, *Ann. Rev. Fluid Mech,vol 33:587-617, 2001.*

[58]J. Katz and A. Plotkin , Low Speed Aerodynamics, *Cambridge University Press, Cambridge, 2001.*

[59]H. Ashley, M. Landahl , Aerodynamics of wings and bodies, *Dover Publications, New York, 1985.*

[60]J.D.Anderson, Fundamentals of Aerodynamics, *Mc-Graw-Hill Science/Engineering, 2001.*

[61]J.J. Bertin, *Aerodynamics for Engineers, Pentice Hall, 4th edition, 2001.*

[62]D.J.Willis, E.R.Israeli, M.Drela, J.Peraire, S.M.Swartz, K.S.Breuer, A computational Framework for Fluid Structure Interaction in Biologically-Inspired Flapping Flight

Appendix

The following images examine the design space sweeps for the baseline cases.

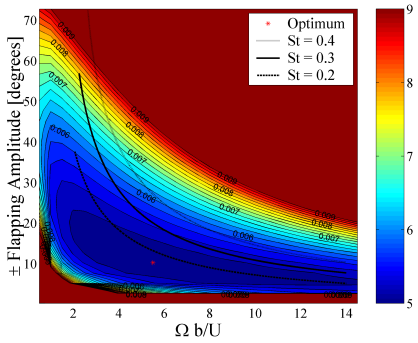

(a) Case 1 : $C_T = 0.0025, C_L = 0.1$

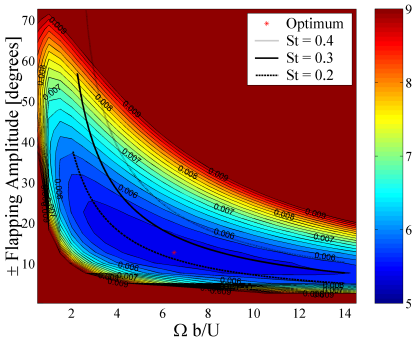

(b) Case 2 : $C_T = 0.005, C_L = 0.1$

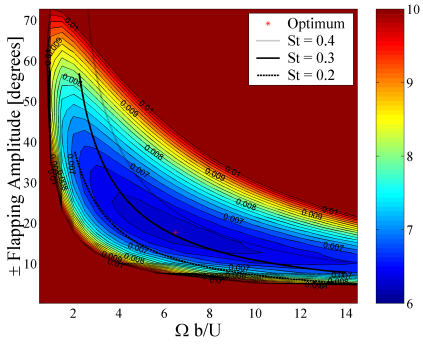

(c) Case 3 : $C_T = 0.01, C_L = 0.1$

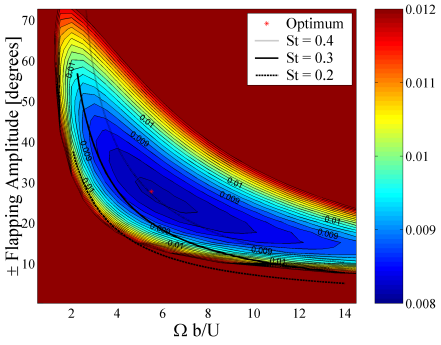

(d) Case 4 : $C_T = 0.02, C_L = 0.1$

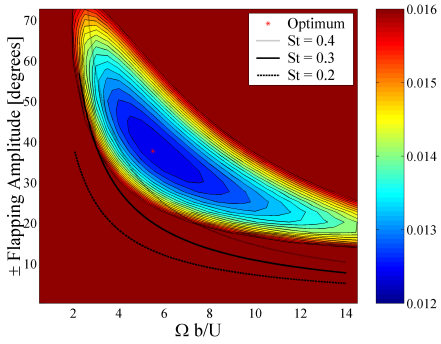

(e) Case 5 : $C_T = 0.04, C_L = 0.1$

Figure 11. An illustration of the HallOpt parameter sweeps for the baseline flapping flight cases. These results are similar to those presented in Hall et al.[50] The results illustrate the coefficient of power for different flapping configurations (colored contours). Also shown on this plot are the lines of constant Strouhal number ($St = 0.2$, $St = 0.3$,and $St = 0.4$). These parameter space sweeps are poerformed for representative flight situations.

The optimal wakes for the baseline cases are shown in figure 12. These wakes are of interest in this paper due to the additional information they may provide when deciphering results which are obtained. For example, wakes with significant thrust production have a strong streamwise and spanwise vorticity component at different stages of the flapping cycle. An understanding of the circulation distribution in each of the lift and thrust producing wakes aids in understanding the potential benefits of formation and ground effect flight.

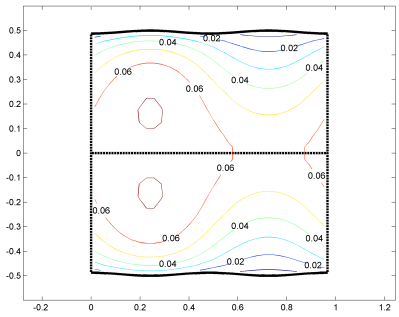

(a) Case 2 : $C_T = 0.005, C_L = 0.1$

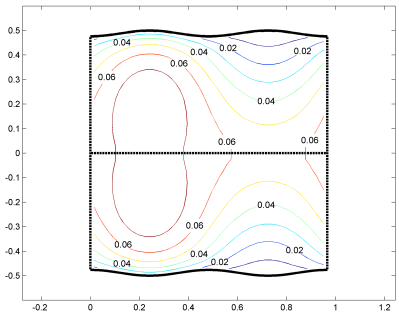

(b) Case 3 : $C_T = 0.01, C_L = 0.1$

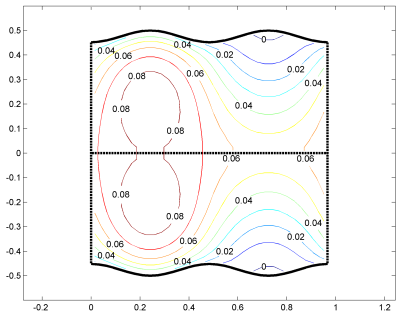

(c) Case 4 : $C_T = 0.02, C_L = 0.1$

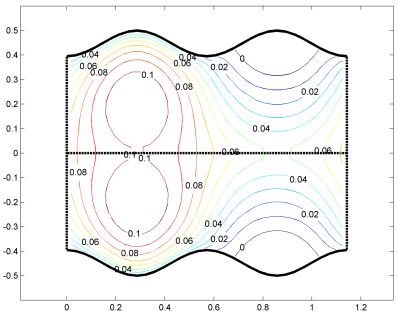

(d) Case 5 : $C_T = 0.04, C_L = 0.1$

Figure 12. An illustration of the optimal HallOpt real wakes for the baseline cases as seen from above. Each of the wakes is capable of producing the same lift coefficient, but different thrust coefficients. It is worth noting that the wakes shapes are different and correspond to the optimal shape for the given degrees of freedom as predicted by the HallOpt code.

The following images examine the design space sweeps for the ground effect cases. In certain plots (low flight heights), the physical boundary of the ground plane is represented using a solid black boundary in the design space sweep. All flapping configurations which violate this constraint are set to have a large flapping power (in order to fill in those violated portions of the design space).

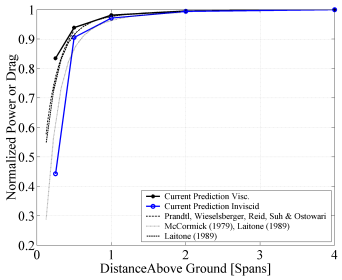

(a) Flight Height vs. Valid Minimum Total Power For $C_T = 0.0025$

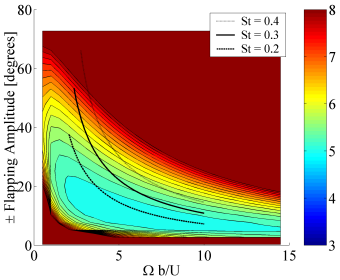

(b) Case 1 : Flight Height ∞,A plot of C_P as a function of amplitude and reduced frequency

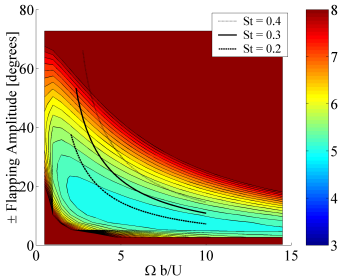

(c) Case 1 : Flight Height = 4.0,A plot of C_P as a function of amplitude and reduced frequency

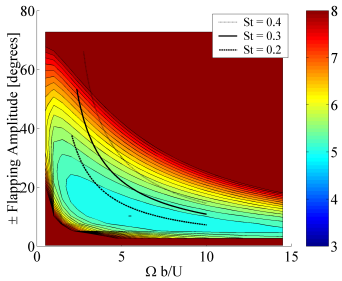

(d) Case 2 : Flight Height = 2.0,A plot of C_P as a function of amplitude and reduced frequency

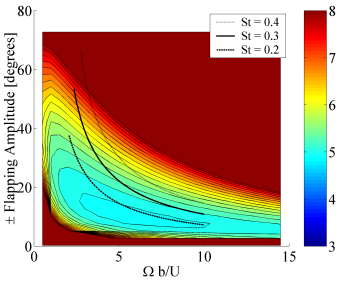

(e) Case 3 : Flight Height = 1.0,A plot of C_P as a function of amplitude and reduced frequency

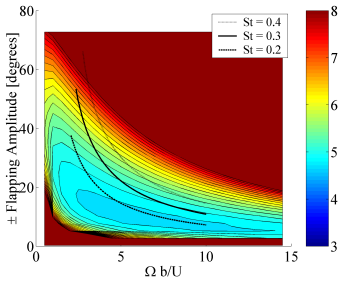

(f) Case 4 : Flight Height = 0.5,A plot of C_P as a function of amplitude and reduced frequency

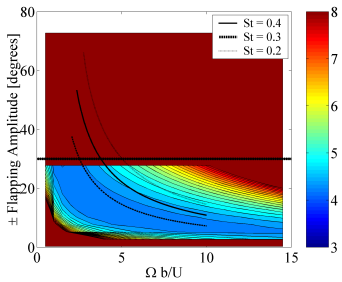

(g) Case 5 : Flight Height = 0.25,A plot of C_P as a function of amplitude and reduced frequency

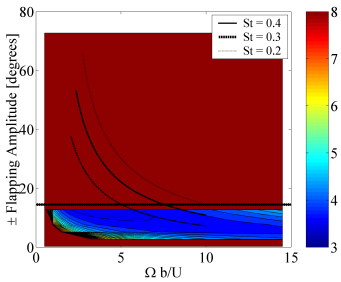

(h) Case 6 : Flight Height = 0.125,A plot of C_P as a function of amplitude and reduced frequency

Figure 13. Design space sweeps for harmonic hinged flappers with a $C_T = 0.0025$ requirement.

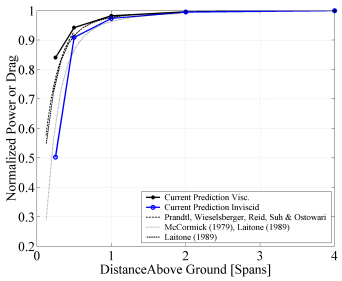

(a) Flight Height vs. Valid Minimum Total Power For $C_T = 0.005$

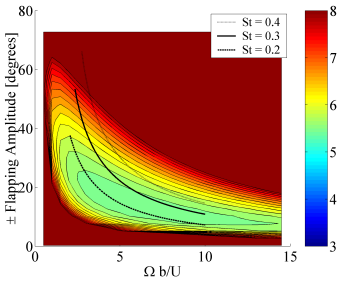

(b) Case 1 : Flight Height ∞,A plot of C_P as a function of amplitude and reduced frequency

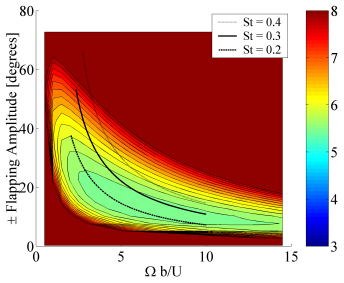

(c) Case 1 : Flight Height = 4.0,A plot of C_P as a function of amplitude and reduced frequency

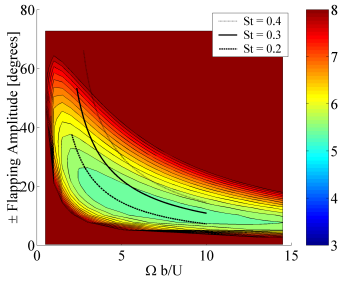

(d) Case 2 : Flight Height = 2.0,A plot of C_P as a function of amplitude and reduced frequency

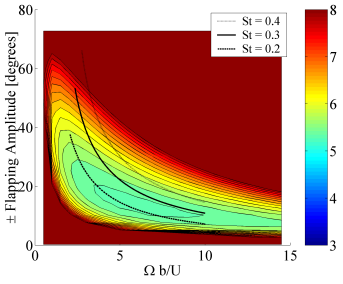

(e) Case 3 : Flight Height = 1.0,A plot of C_P as a function of amplitude and reduced frequency

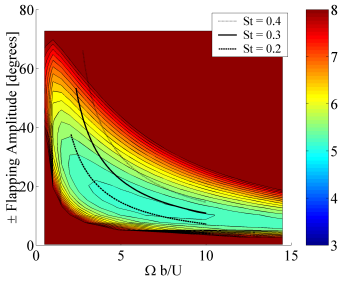

(f) Case 4 : Flight Height = 0.5,A plot of C_P as a function of amplitude and reduced frequency

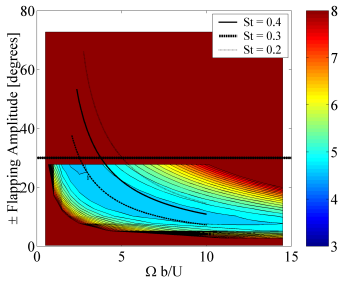

(g) Case 5 : Flight Height = 0.25,A plot of C_P as a function of amplitude and reduced frequency

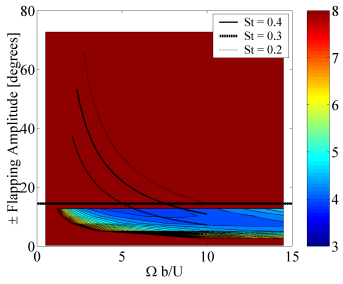

(h) Case 6 : Flight Height = 0.125,A plot of C_P as a function of amplitude and reduced frequency

Figure 14. Design space sweeps for harmonic hinged flappers with a $C_T = 0.005$ requirement.

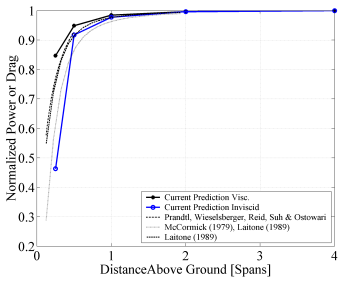

(a) Flight Height vs. Valid Minimum Total Power For $C_T = 0.01$

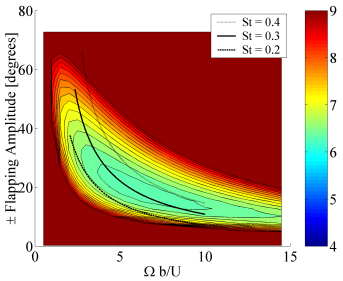

(b) Case 1 : Flight Height ∞,A plot of C_P as a function of amplitude and reduced frequency

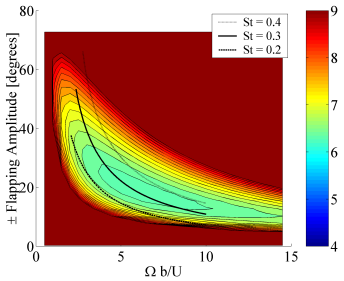

(c) Case 1 : Flight Height = 4.0,A plot of C_P as a function of amplitude and reduced frequency

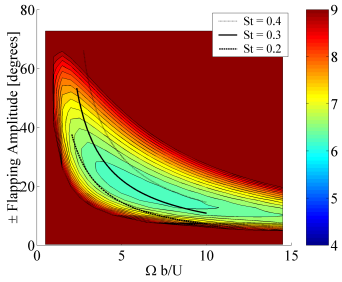

(d) Case 2 : Flight Height = 2.0,A plot of C_P as a function of amplitude and reduced frequency

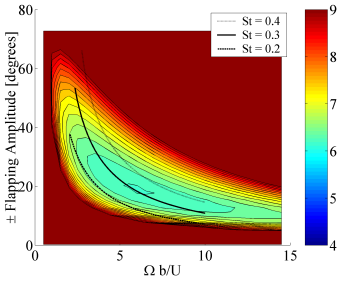

(e) Case 3 : Flight Height = 1.0,A plot of C_P as a function of amplitude and reduced frequency

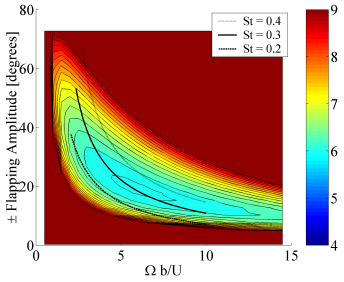

(f) Case 4 : Flight Height = 0.5,A plot of C_P as a function of amplitude and reduced frequency

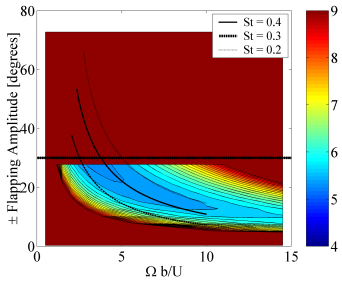

(g) Case 5 : Flight Height = 0.25,A plot of C_P as a function of amplitude and reduced frequency

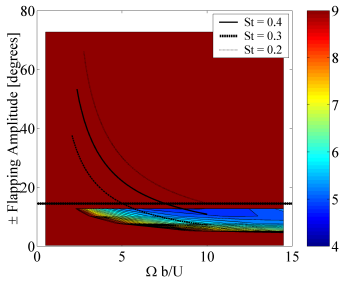

(h) Case 6 : Flight Height = 0.125,A plot of C_P as a function of amplitude and reduced frequency

Figure 15. Design space sweeps for harmonic hinged flappers with a $C_T = 0.01$ requirement.

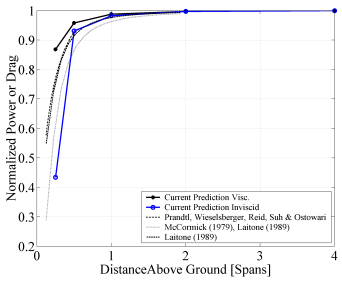

(a) Flight Height vs. Valid Minimum Total Power For $C_T = 0.02$

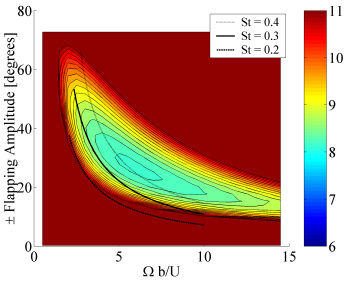

(b) Case 1 : Flight Height ∞,A plot of C_P as a function of amplitude and reduced frequency

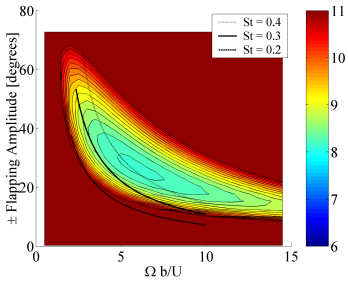

(c) Case 1 : Flight Height = 4.0,A plot of C_P as a function of amplitude and reduced frequency

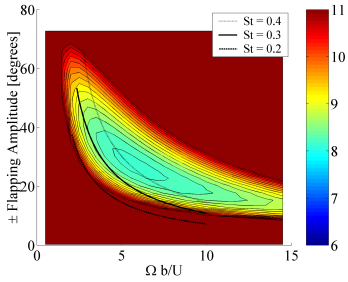

(d) Case 2 : Flight Height = 2.0,A plot of C_P as a function of amplitude and reduced frequency

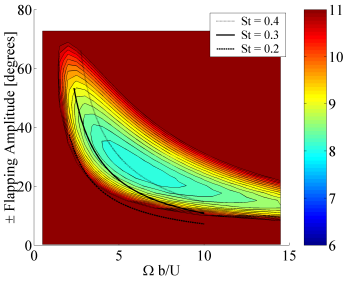

(e) Case 3 : Flight Height = 1.0,A plot of C_P as a function of amplitude and reduced frequency

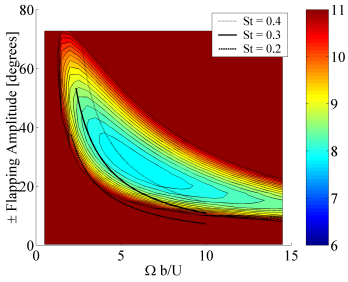

(f) Case 4 : Flight Height = 0.5,A plot of C_P as a function of amplitude and reduced frequency

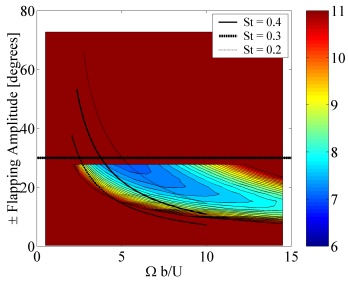

(g) Case 5 : Flight Height = 0.25,A plot of C_P as a function of amplitude and reduced frequency

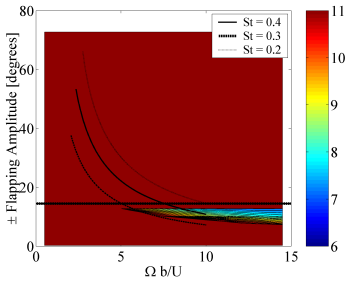

(h) Case 6 : Flight Height = 0.125,A plot of C_P as a function of amplitude and reduced frequency

Figure 16. Design space sweeps for harmonic hinged flappers with a $C_T = 0.02$ requirement.

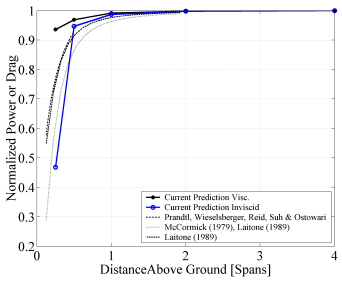

(a) Flight Height vs. Valid Minimum Total Power For $C_T = 0.04$

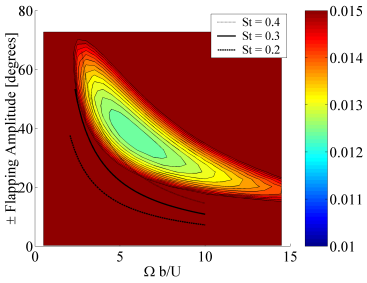

(b) Case 1 : Flight Height ∞,A plot of C_P as a function of amplitude and reduced frequency

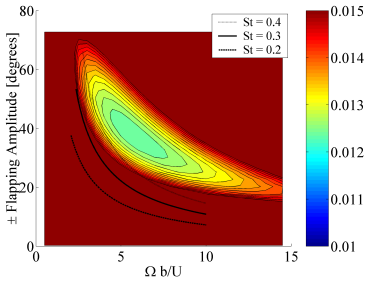

(c) Case 1 : Flight Height = 4.0,A plot of C_P as a function of amplitude and reduced frequency

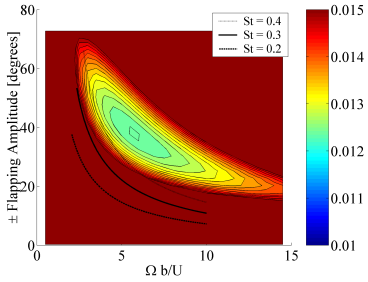

(d) Case 2 : Flight Height = 2.0,A plot of C_P as a function of amplitude and reduced frequency

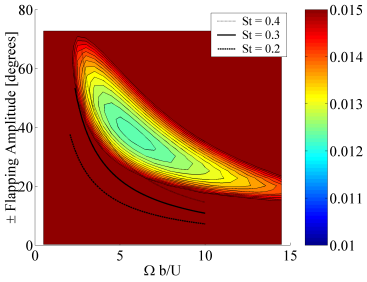

(e) Case 3 : Flight Height = 1.0,A plot of C_P as a function of amplitude and reduced frequency

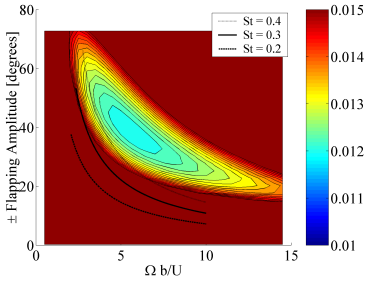

(f) Case 4 : Flight Height = 0.5,A plot of C_P as a function of amplitude and reduced frequency

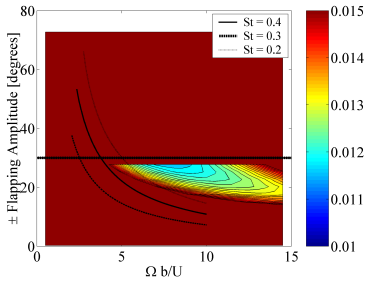

(g) Case 5 : Flight Height = 0.25,A plot of C_P as a function of amplitude and reduced frequency

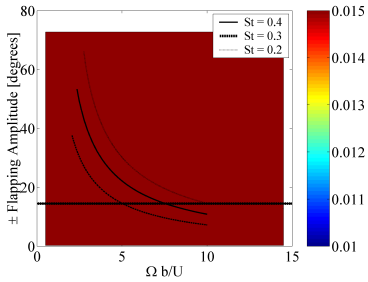

(h) Case 6 : Flight Height = 0.125,A plot of C_P as a function of amplitude and reduced frequency

Figure 17. Design space sweeps for harmonic hinged flappers with a $C_T = 0.04$ requirement.

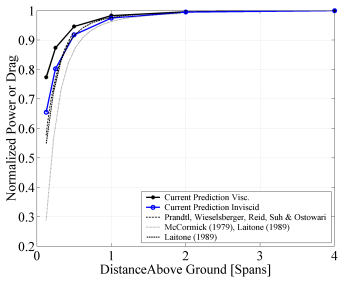

(a) Flight Height vs. Valid Minimum Total Power

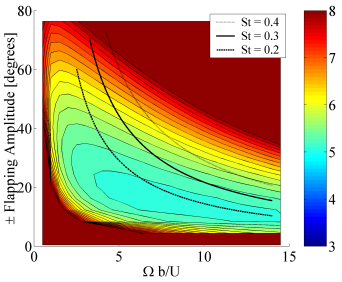

(b) Case 1 : Flight Height ∞,A plot of C_P as a function of amplitude and reduced frequency

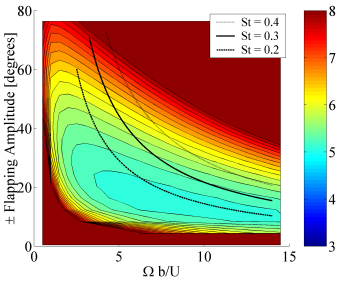

(c) Case 1 : Flight Height = 4.0,A plot of C_P as a function of amplitude and reduced frequency

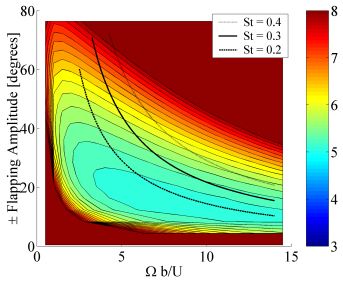

(d) Case 2 : Flight Height = 2.0,A plot of C_P as a function of amplitude and reduced frequency

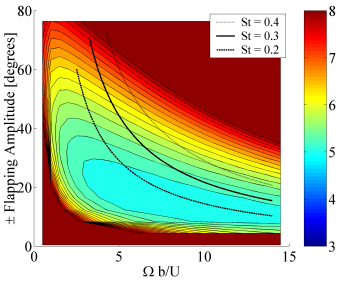

(e) Case 3 : Flight Height = 1.0,A plot of C_P as a function of amplitude and reduced frequency

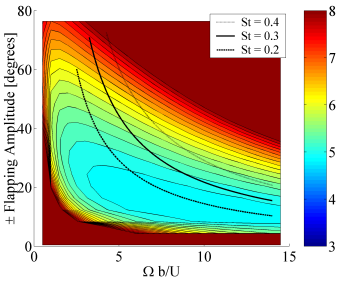

(f) Case 4 : Flight Height = 0.5,A plot of C_P as a function of amplitude and reduced frequency

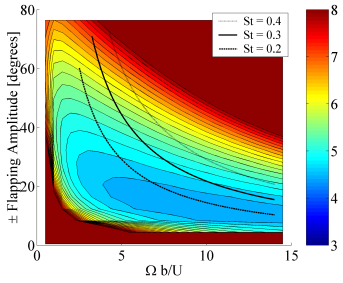

(g) Case 5 : Flight Height = 0.25,A plot of C_P as a function of amplitude and reduced frequency

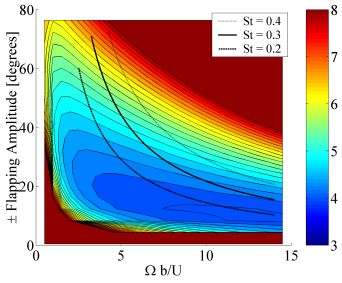

(h) Case 6 : Flight Height = 0.125,A plot of C_P as a function of amplitude and reduced frequency

Figure 18. Design space sweeps for harmonic hinged flappers with a $C_T = 0.0025$ requirement. In this case the flapping is performed with a positive dihedral angle throughout the flapping cycle.

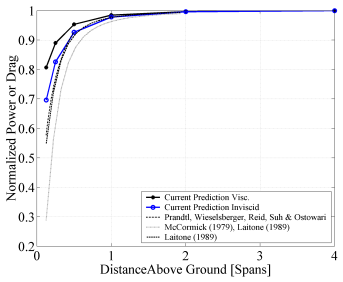

(a) Flight Height vs. Valid Minimum Total Power

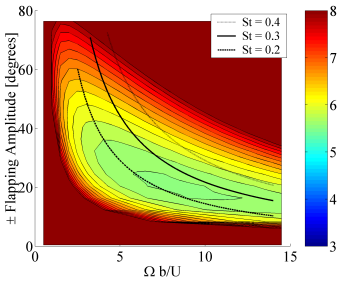

(b) Case 1 : Flight Height ∞,A plot of C_P as a function of amplitude and reduced frequency

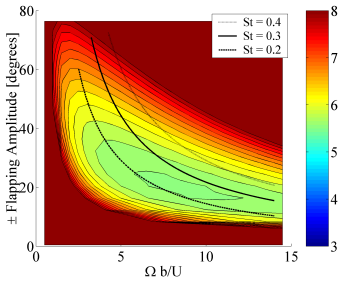

(c) Case 1 : Flight Height = 4.0,A plot of C_P as a function of amplitude and reduced frequency

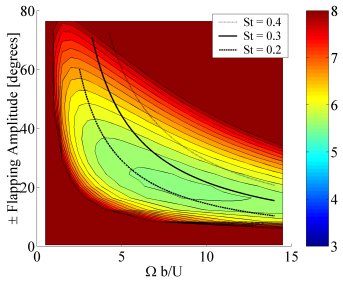

(d) Case 2 : Flight Height = 2.0,A plot of C_P as a function of amplitude and reduced frequency

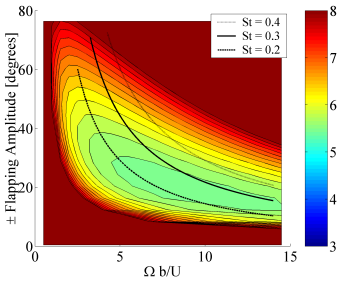

(e) Case 3 : Flight Height = 1.0,A plot of C_P as a function of amplitude and reduced frequency

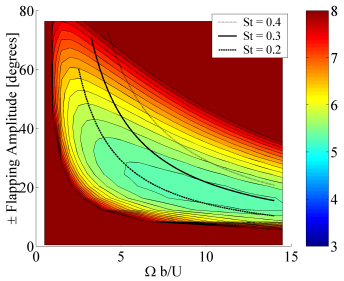

(f) Case 4 : Flight Height = 0.5,A plot of C_P as a function of amplitude and reduced frequency

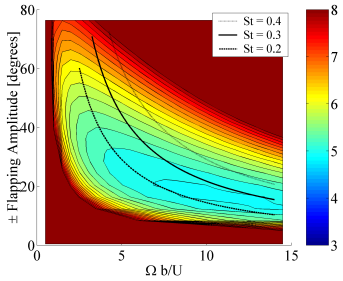

(g) Case 5 : Flight Height = 0.25,A plot of C_P as a function of amplitude and reduced frequency

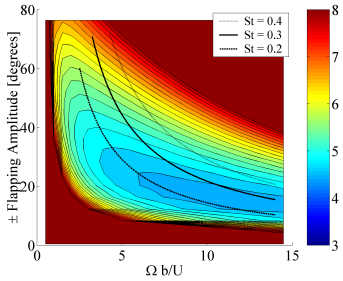

(h) Case 6 : Flight Height = 0.125,A plot of C_P as a function of amplitude and reduced frequency

Figure 19. Design space sweeps for harmonic hinged flappers with a $C_T = 0.005$ requirement. In this case the flapping is performed with a positive dihedral angle throughout the flapping cycle.

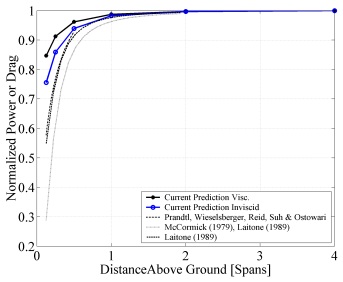

(a) Flight Height vs. Valid Minimum Total Power

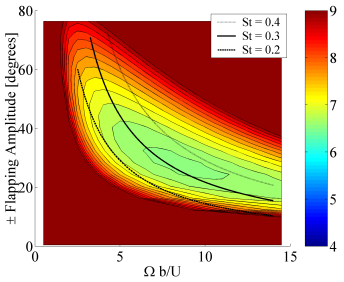

(b) Case 1 : Flight Height ∞,A plot of C_P as a function of amplitude and reduced frequency

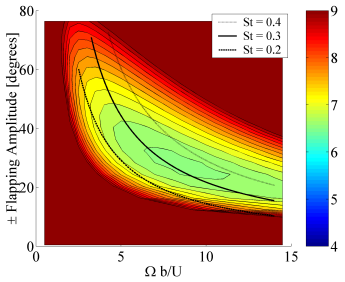

(c) Case 1 : Flight Height = 4.0,A plot of C_P as a function of amplitude and reduced frequency

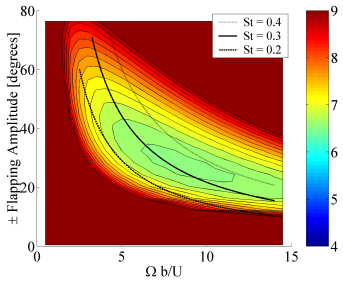

(d) Case 2 : Flight Height = 2.0,A plot of C_P as a function of amplitude and reduced frequency

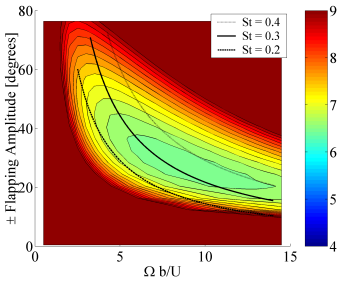

(e) Case 3 : Flight Height = 1.0,A plot of C_P as a function of amplitude and reduced frequency

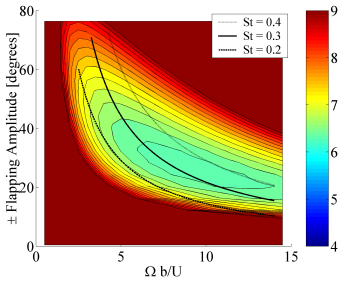

(f) Case 4 : Flight Height = 0.5,A plot of C_P as a function of amplitude and reduced frequency

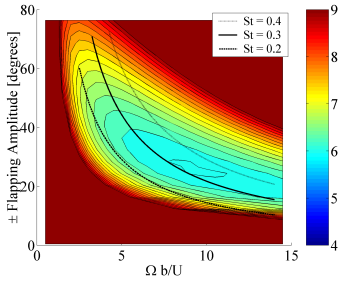

(g) Case 5 : Flight Height = 0.25,A plot of C_P as a function of amplitude and reduced frequency

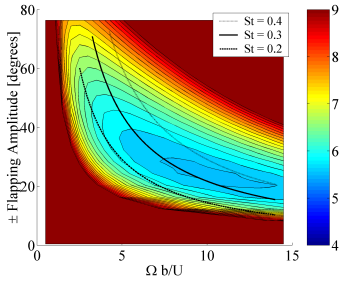

(h) Case 6 : Flight Height = 0.125,A plot of C_P as a function of amplitude and reduced frequency

Figure 20. Design space sweeps for harmonic hinged flappers with a $C_T = 0.01$ requirement. In this case the flapping is performed with a positive dihedral angle throughout the flapping cycle.

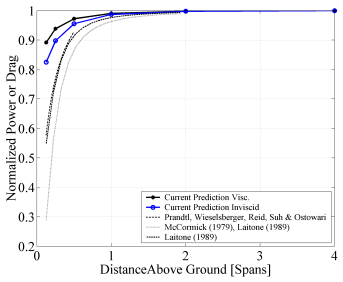

(a) Flight Height vs. Valid Minimum Total Power

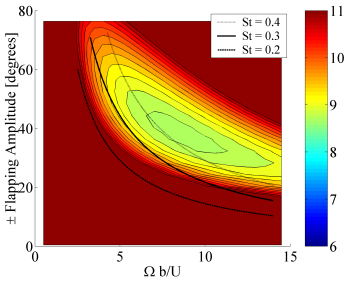

(b) Case 1 : Flight Height ∞,A plot of C_P as a function of amplitude and reduced frequency

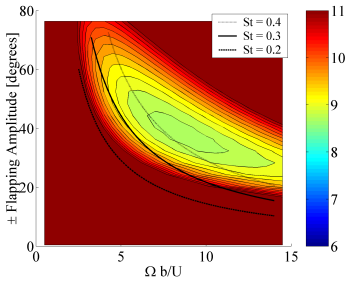

(c) Case 1 : Flight Height = 4.0,A plot of C_P as a function of amplitude and reduced frequency

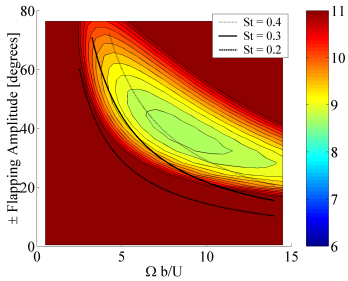

(d) Case 2 : Flight Height = 2.0,A plot of C_P as a function of amplitude and reduced frequency

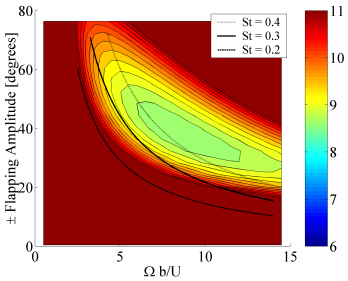

(e) Case 3 : Flight Height = 1.0,A plot of C_P as a function of amplitude and reduced frequency

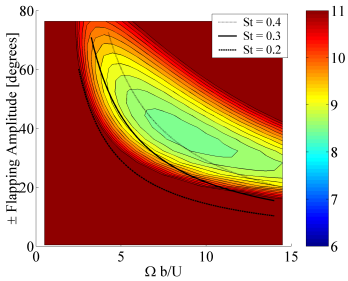

(f) Case 4 : Flight Height = 0.5,A plot of C_P as a function of amplitude and reduced frequency

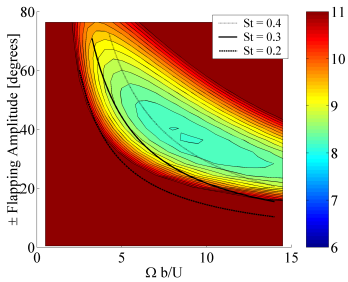

(g) Case 5 : Flight Height = 0.25,A plot of C_P as a function of amplitude and reduced frequency

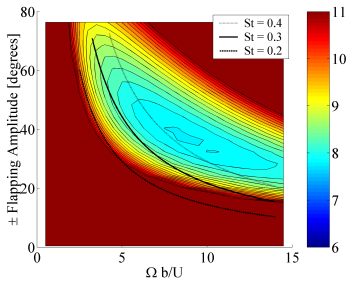

(h) Case 6 : Flight Height = 0.125,A plot of C_P as a function of amplitude and reduced frequency

Figure 21. Design space sweeps for harmonic hinged flappers with a $C_T = 0.02$ requirement. In this case the flapping is performed with a positive dihedral angle throughout the flapping cycle.

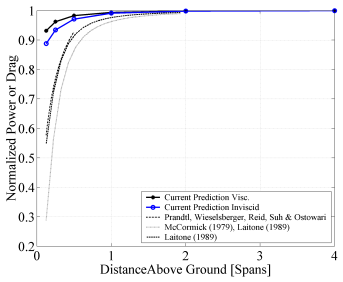

(a) Flight Height vs. Valid Minimum Total Power

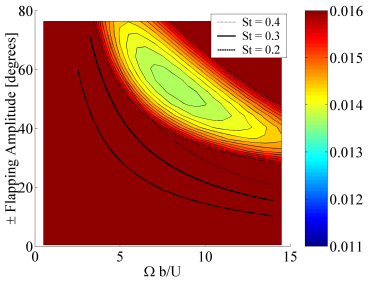

(b) Case 1 : Flight Height ∞,A plot of C_P as a function of amplitude and reduced frequency

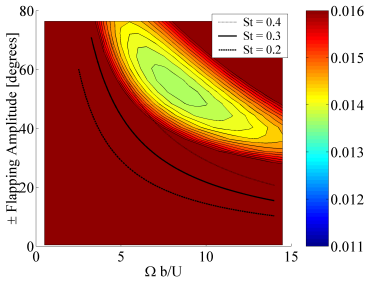

(c) Case 1 : Flight Height = 4.0,A plot of C_P as a function of amplitude and reduced frequency

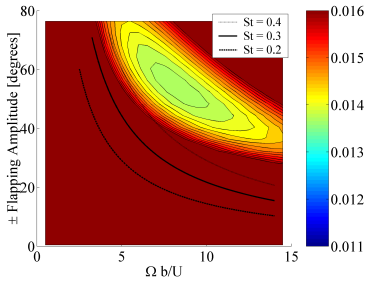

(d) Case 2 : Flight Height = 2.0,A plot of C_P as a function of amplitude and reduced frequency

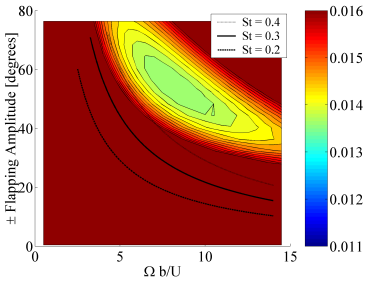

(e) Case 3 : Flight Height = 1.0,A plot of C_P as a function of amplitude and reduced frequency

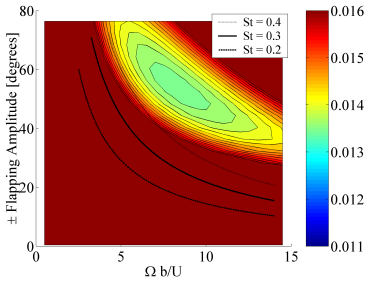

(f) Case 4 : Flight Height = 0.5,A plot of C_P as a function of amplitude and reduced frequency

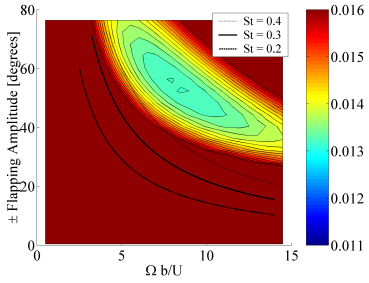

(g) Case 5 : Flight Height = 0.25,A plot of C_P as a function of amplitude and reduced frequency

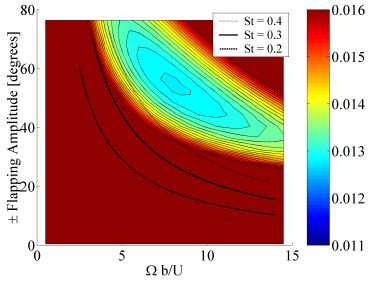

(h) Case 6 : Flight Height = 0.125, A plot of C_P as a function of amplitude and reduced frequency

Figure 22. Design space sweeps for harmonic hinged flappers with a $C_T = 0.04$ requirement. In this case the flapping is performed with a positive dihedral angle throughout the flapping cycle.

The following images examine the design space sweeps for the formation flight cases.

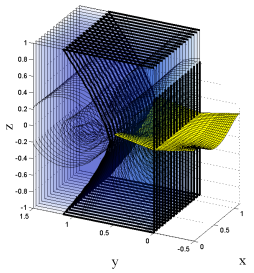

(a) $C_T = 0.0025$

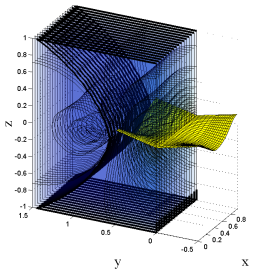

(b) $C_T = 0.005$

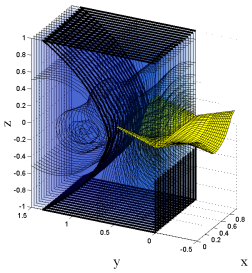

(c) $C_T = 0.010$

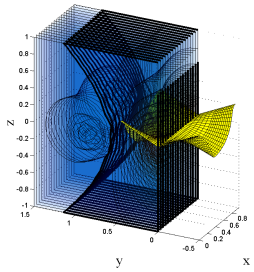

(d) $C_T = 0.020$

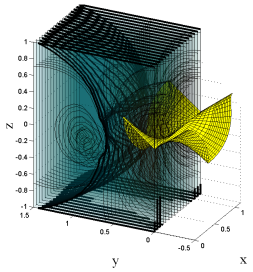

(e) $C_T = 0.040$

Figure 23. A series of cluster plots of data illustrating the design space sweep over a three dimensional cube of following bird positions. In each of the above images, the power required for producing the specified lift and thrust for the following wake flapping vehicle is computed. The plot above illustrates this power computation as a function of the mid-line of the wing at the start of the downstroke. In other words, the power of a following bird flapping in space-phase with the lead bird would be plotted on the first vertical plane of the cube, with (x, z) position defined by the body location. The power is plotted where the body of the bird is located as the beginning of downstroke.

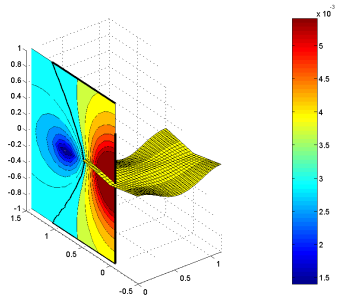

(a) $C_T = 0.0025$, Following bird in phase with the lead bird

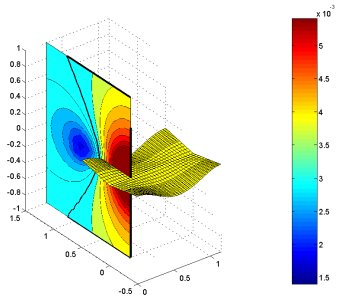

(b) $C_T = 0.0025$, Following Bird out of phase by $\frac{\pi}{2}$ from the lead bird

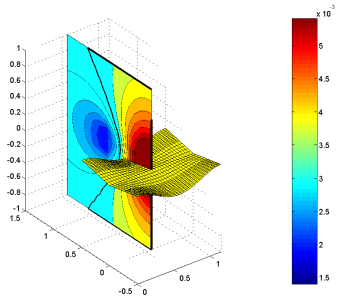

(c) $C_T = 0.0025$, following bird out of phase by π from the lead bird flapping

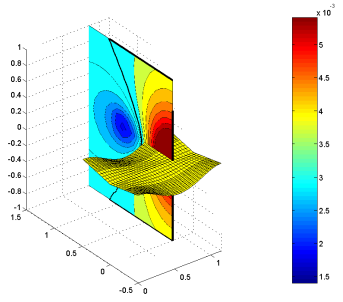

(d) $C_T = 0.0025$, following bird out of phase by $-\frac{\pi}{2}$ from the lead bird

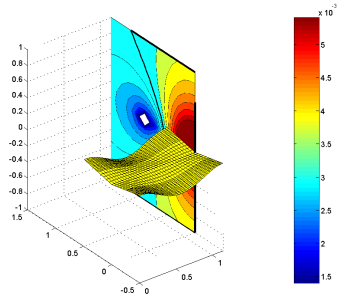

(e) $C_T = 0.0025$, following bird in phase with the lead bird

Figure 24. Contour slices for $C_T = 0.0025$, $C_L = 0.1$, representing where the energy saving zones for flapping are located. In these plots, a region of low power represents the position of the mid-line of the body, when the bird starts its flapping cycle. The dark/bold contour in this plot indicates the breakeven point of no energy savings and no energy loss.

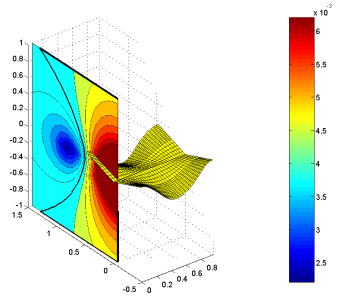

(a) $C_T = 0.005$, $C_L = 0.1$, Following bird in phase with the lead bird

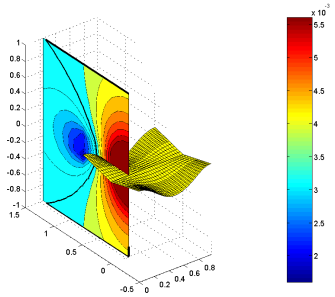

(b) $C_T = 0.005$, $C_L = 0.1$, Following Bird out of phase by $\frac{\pi}{2}$ from the lead bird

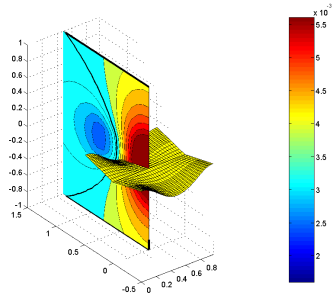

(c) $C_T = 0.005$, $C_L = 0.1$, following bird out of phase by π from the lead bird flapping

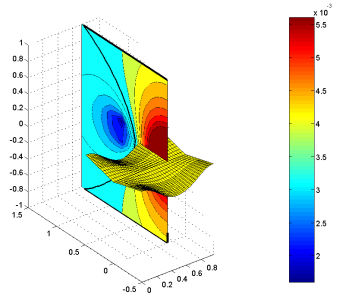

(d) $C_T = 0.005$, $C_L = 0.1$,following bird out of phase by $-\frac{\pi}{2}$ from the lead bird

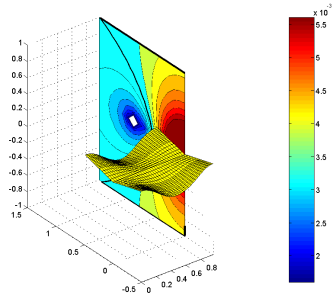

(e) $C_T = 0.005$, $C_L = 0.1$, following bird in phase with the lead bird

Figure 25. Contour slices for $C_T = 0.005$, $C_L = 0.1$, representing where the energy saving zones for flapping are located. In these plots, a region of low power represents the position of the mid-line of the body, when the bird starts its flapping cycle.

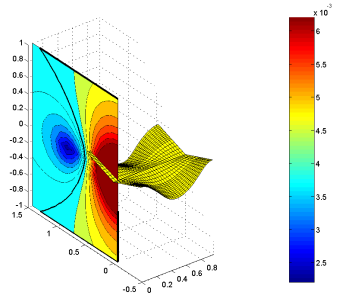

(a) $C_T = 0.01$, $C_L = 0.1$, Following bird in phase with the lead bird

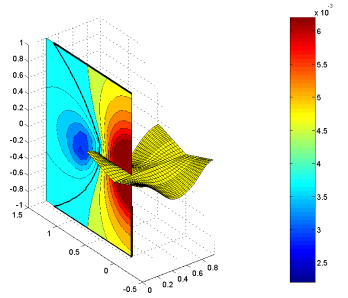

(b) $C_T = 0.01$, $C_L = 0.1$,Following Bird out of phase by $\frac{\pi}{2}$ from the lead bird

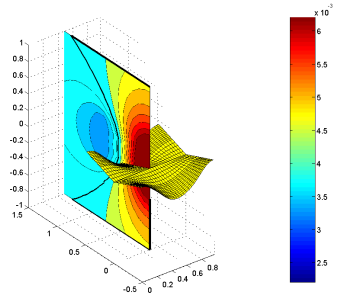

(c) $C_T = 0.01$, $C_L = 0.1$, following bird out of phase by π from the lead bird flapping

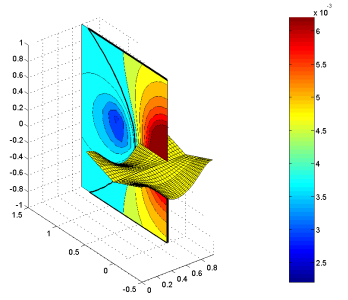

(d) $C_T = 0.01$, $C_L = 0.1$,following bird out of phase by $-\frac{\pi}{2}$ from the lead bird

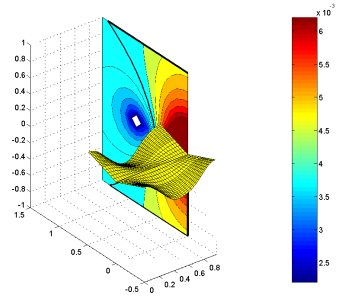

(e) $C_T = 0.01$, $C_L = 0.1$, following bird in phase with the lead bird

Figure 26. Contour slices for $C_T = 0.01$, $C_L = 0.1$, representing where the energy saving zones for flapping are located. In these plots, a region of low power represents the position of the mid-line of the body, when the bird starts its flapping cycle. At this stage in the analysis, it is possible to see a preference for the flapping motions of the following bird which mimic the lead bird (in space). This can be seen from the clustering of the lower power values near the start and end of the wake period.

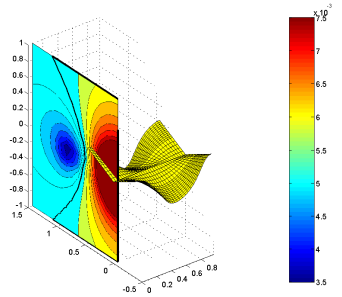

(a) $C_T = 0.02$, $C_L = 0.1$, Following bird in phase with the lead bird

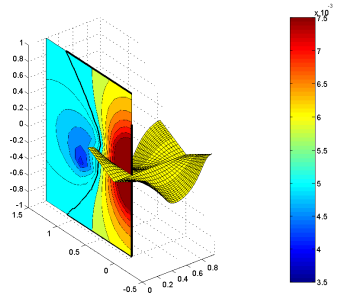

(b) $C_T = 0.02$, $C_L = 0.1$, Following Bird out of phase by $\frac{\pi}{2}$ from the lead bird

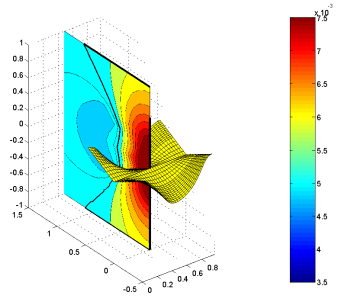

(c) $C_T = 0.02$, $C_L = 0.1$, following bird out of phase by π from the lead bird flapping

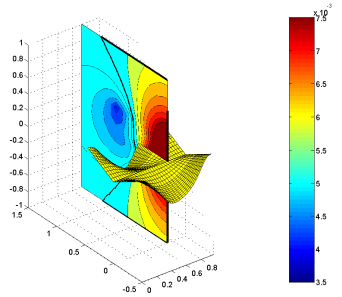

(d) $C_T = 0.02$, $C_L = 0.1$, following bird out of phase by $-\frac{\pi}{2}$ from the lead bird

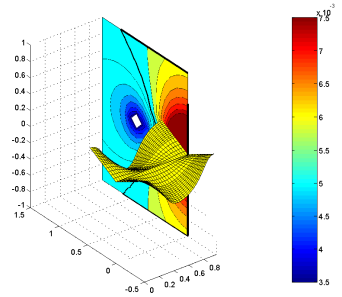

(e) $C_T = 0.02$, $C_L = 0.1$, following bird in phase with the lead bird

Figure 27. Contour slices for $C_T = 0.02$, $C_L = 0.1$, representing where the energy saving zones for flapping are located. In these plots, a region of low power represents the position of the mid-line of the body, when the bird starts its flapping cycle. At this point, it is evident that in phase flapping is more beneficial than out of phase flapping. Meaning, that the following bird should try to fly in the wake of the lead bird exactly capturing the downwash at all points in the flapping cycle.

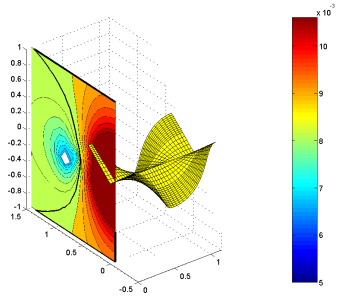

(a) $C_T = 0.04$, $C_L = 0.1$, Following bird in phase with the lead bird

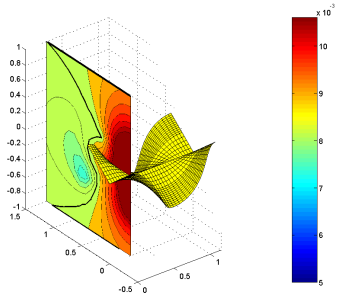

(b) $C_T = 0.04$, $C_L = 0.1$, Following Bird out of phase by $\frac{\pi}{2}$ from the lead bird

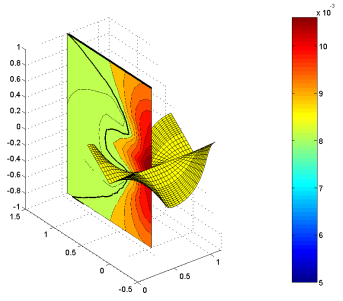

(c) $C_T = 0.04$, $C_L = 0.1$, following bird out of phase by π from the lead bird flapping

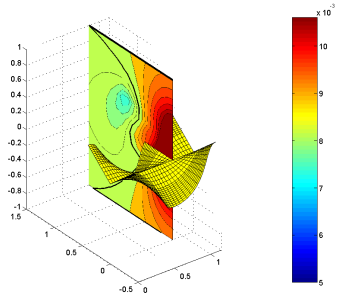

(d) $C_T = 0.04$, $C_L = 0.1$, following bird out of phase by $-\frac{\pi}{2}$ from the lead bird

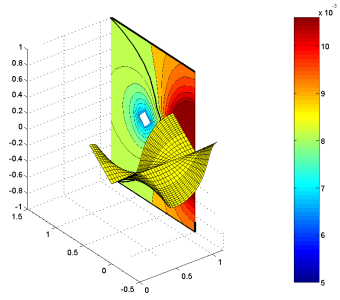

(e) $C_T = 0.04$, $C_L = 0.1$, following bird in phase with the lead bird

Figure 28. Contour slices for $C_T = 0.04$, $C_L = 0.1$, representing where the energy saving zones for flapping are located. In these plots, a region of low power represents the position of the mid-line of the body, when the bird starts its flapping cycle. At this stage in the analysis, it is possible to see a preference for the flapping motions of the following bird which mimic the lead bird (in space). This can be seen from the clustering of the lower power values near the start and end of the wake period. In addition, we see that the dividing line between energy savings and energy penalty tends to be shifting spanwise at the mid-cycle position, implying that flying spatially out of phase by π radians is not a recommended feature.